

Controlling Sawtooth Oscillations in Tokamak Plasmas

IT Chapman

EURATOM/CCFE Fusion Association, Culham Science Centre, Abingdon,
Oxfordshire OX14 3DB, United Kingdom

E-mail: ian.chapman@ccfe.ac.uk

Abstract.

The sawtooth instability in tokamak plasmas results in a periodic reorganization of the core plasma. A typical sawtooth cycle consists of a quiescent period, during which the plasma density and temperature increase, followed by the growth of a helical magnetic perturbation, which in turn is followed by a rapid collapse of the central pressure. The stabilizing effects of fusion-born α particles are likely to lead to long sawtooth periods in burning plasmas. However, sawteeth with long quiescent periods have been observed to result in the early triggering of neo-classical tearing modes (NTMs) at low plasma pressure, which can, in turn, significantly degrade confinement. Consequently, recent experiments have identified various methods to deliberately control sawtooth oscillations in an attempt to avoid seeding NTMs whilst retaining the benefits of small, frequent sawteeth, such as the prevention of core impurity accumulation. Sawtooth control actuators include current drive schemes, such as electron cyclotron current drive, and tailoring the fast ion population in the plasma using neutral beam injection or ion cyclotron resonance heating.

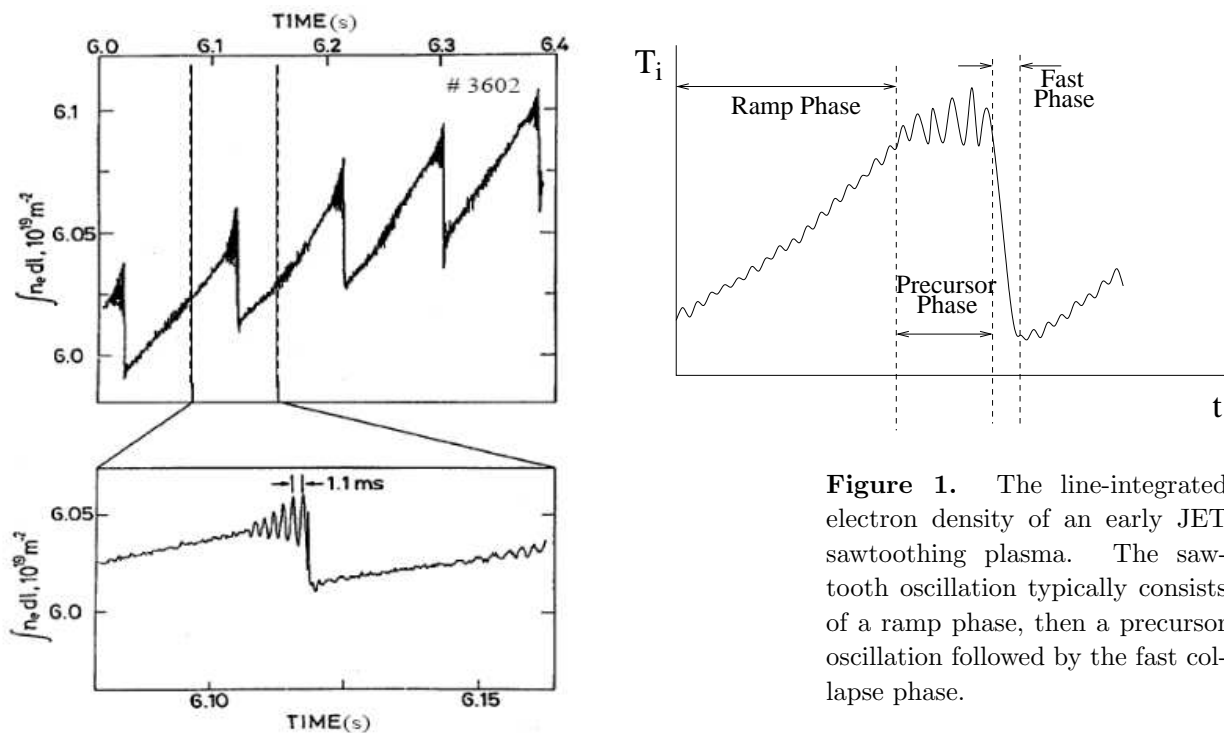


Figure 1. The line-integrated electron density of an early JET sawtoothing plasma. The sawtooth oscillation typically consists of a ramp phase, then a precursor oscillation followed by the fast collapse phase.

1. Introduction

Tokamak plasmas are observed to be susceptible to a variety of large-scale instabilities which can degrade the plasma confinement. The stability boundaries of these large plasma instabilities determine the safe operating regime of the tokamak. The sawtooth is one such macroscopic instability, though it rarely leads to a termination of a discharge despite affecting a significant volume of the plasma [1].

Sawtooth oscillations are periodic relaxations of the core plasma density and temperature [2, 3]. These periodic redistributions of the core plasma surrounding the magnetic axis were first observed in 1974 [4] and have subsequently been seen on every tokamak. A typical sawtooth cycle is depicted in figure (1) which shows the three phases: (i) the sawtooth ramp phase during which the plasma density and temperature increase approximately linearly with respect to time; (ii) the precursor phase, during which a helical magnetic perturbation grows until (iii) the fast collapse phase, when the density and temperature drop rapidly. When a sawtooth crash occurs, hot electrons transport rapidly across flux surfaces to a cooler region of plasma, such that the temperature profile is flattened. Figure (2) shows that a rapid drop in the core temperature (here measured by the soft X-ray emission) is accompanied by heating of the edge plasma. The temperature is observed to remain constant at the *inversion radius*. Recently, two-dimensional measurement of electron temperature fluctuations [5, 6] has provided imaging of the collective behaviour of the crash, whereby the hot plasma core is expelled through a poloidally localised point as magnetic reconnection occurs, as illustrated in figure 3.

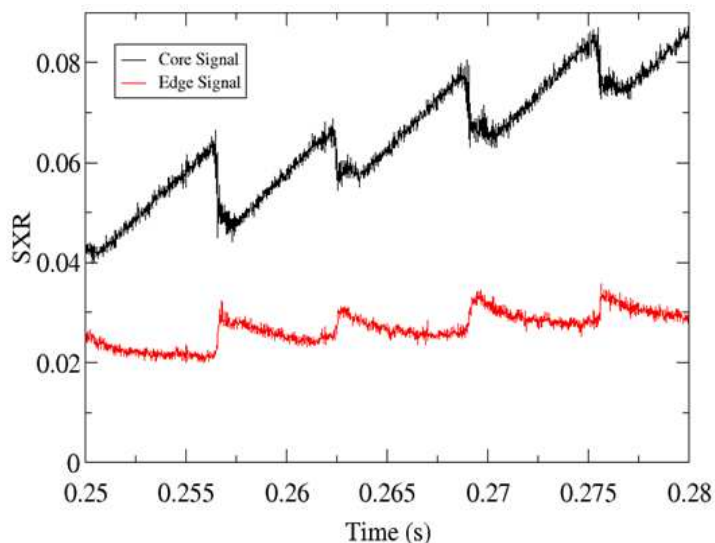


Figure 2. The measured Soft X-ray signal during MAST discharge 8360. At each sawtooth crash the central soft X-ray emission exhibits a rapid decrease, whilst concurrently the edge plasma shows an increase in emission.

In order to control sawteeth, it is most important to understand the second phase in the cycle - the trigger of the instability growth. Since this onset of instability can be understood in terms of linear stability thresholds, the theoretical considerations of such stability are discussed in detail in section 2. Experiments have shown (see [1] and references therein) that the precursor oscillation has the topology of the $n = m = 1$ internal kink mode – a fundamental magnetohydrodynamic (MHD) oscillation of the form $\xi \sim \exp(im\theta - in\phi)$ where m and n are the poloidal and toroidal mode number respectively, ξ is the perturbation to the plasma and θ and ϕ are the poloidal and toroidal angles. The ideal internal kink displacement takes the form of a tilt and a shift of the core plasma. Since the sawtooth crash is usually accompanied by an $n = m = 1$ displacement of the plasma (although it should be noted that tokamak plasmas do sometimes experience precursorless sawteeth [7]), there have been many studies concerning the stability of this mode and its connection to the sawtooth event. In order to model the behaviour of the kink mode, the collective motion of the collisional thermal particles can be adequately described by MHD. However, the dynamics of energetic particles (for instance born due to Ion Cyclotron Resonance Heating (ICRH) or Neutral Beam Injection (NBI), or α particles from fusion reactions) are described using the guiding-centre approximation, whereby the fast gyration of the energetic particles along a helical path is approximated as a drifting trajectory. By so doing, the various stabilising and destabilising influences upon the internal kink mode can be assessed by using the energy principle. In essence this says that if a physically allowable perturbation lowers the potential energy of the plasma, then the mode is unstable [2].

Small sawteeth which have an inversion radius less than 40% of the minor radius and a temperature drop of the order of a fraction of a keV can be tolerated by the

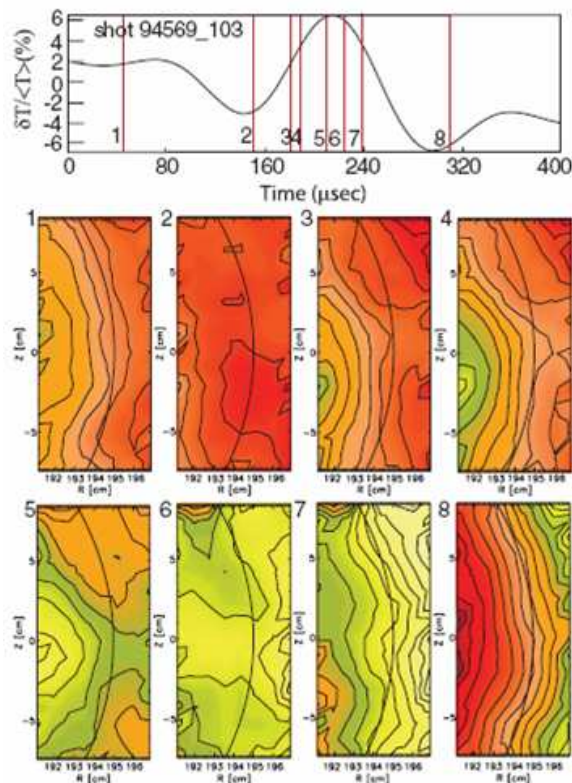


Figure 3. 2D images of the sawtooth crash from Electron cyclotron emission imaging at the low-field side mid-plane on TEXTOR. As the hot spot swells as shown in frames 3 and 4, a sharp temperature point is growing and crosses beyond the inversion radius (marked by the black arc). Eventually, the temperature point leads to the reconnection. Initially, it forms an X-point in the poloidal plane (frame 5), and heat starts to flow to the outside through a small opening. The initial heat flow is highly collective, and the opening increases up to 15 cm. At the end, the heat is accumulated outside the inversion radius, and the poloidal symmetry is recovered. Reprinted figure with permission from Park *et al* Phys Rev. Lett., **96** 195003 (2006) [5]. Copyright 2006 by the American Physical Society

plasma [8]. Indeed, such small sawteeth can be beneficial in preventing accumulation of helium ash in the core plasma [9]. Conversely, long period sawteeth with an inversion radius approaching half of the minor radius and a temperature collapse of the order of a keV can couple to other more deleterious instabilities. It has been shown that plasmas with long period sawteeth are more susceptible to Neo-classical Tearing Modes (NTMs) [10–17] (see figure (4)) and to Edge Localised Modes (ELMs) [18]. NTMs are resistive tearing modes which are sustained by a perturbation to the bootstrap current (a current caused by pressure gradients in the plasma) [19–21]. Unlike sawteeth, NTMs are long-living instabilities and their presence degrades both the plasma energy and the angular momentum [15] and can even lead to terminations, as in figure (4). Figure (5) shows how the critical β_N at which an $m/n = 3/2$ NTM is triggered varies with respect to the sawtooth period in JET plasmas. It is evident that as the sawtooth period lengthens,

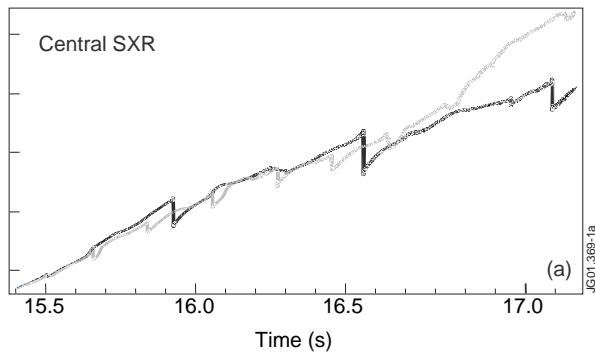
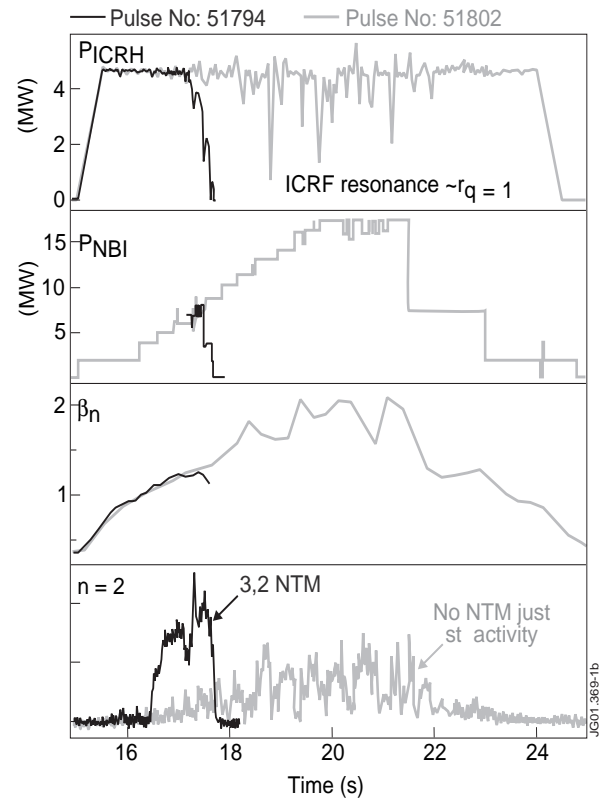


Figure 4. Two similar JET discharges with 2.4T, 2.4MA and 4.5MW of ICRF power. In shot 51974, the ICRF antenna phasing is altered such that the sawtooth period is lengthened. This increased sawtooth period leads to the triggering of $n = 2$ MHD activity which causes a termination of the discharge. Reprinted figure with permission from Sauter *et al* Phys Rev. Lett., **88** 105001 (2002) [12]. Copyright 2002 by the American Physical Society



the NTMs are triggered at lower β_N , hence limiting the plasma performance achievable. Meanwhile, ELMs are short bursts of the plasma edge which cause degradation of the global plasma density and energy as well as erosion of plasma-facing wall components.

It is predicted that fusion-born α particles will lead to very long sawtooth periods in ITER [22–24]. Furthermore, alpha-tail production with ICRF heating of He^4 -beam ions in JET confirmed that the energetic α particles result in “monster” sawteeth [25, 26], which are loosely defined as sawteeth with periods longer than the energy confinement time, and hence saturated central plasma temperature. Consequently, in recent years, much effort has been invested in the control of sawteeth. The two approaches to sawtooth control are to attempt to suppress sawteeth for many energy confinement times (ie *stabilise* the kink mode) or to deliberately decrease the sawtooth period (ie *destabilise* the kink mode). Naturally, the necessity to control sawteeth can be avoided by adopting an advanced tokamak scenario, such as a reversed shear steady-state scenario [27–29] or the hybrid scenario [30, 31] where $q > 1$ (q is the safety factor, measuring the inverse average pitch angle of the magnetic field lines). However, the baseline scenario in ITER is predicated upon the ability of the sawteeth to reverse the on-axis accumulation of higher- Z impurities that would otherwise cause degradation of energy confinement due to impurity radiation. The approach currently adopted for sawtooth control in baseline scenarios in ITER is to deliberately destabilise the internal kink mode to give frequent,

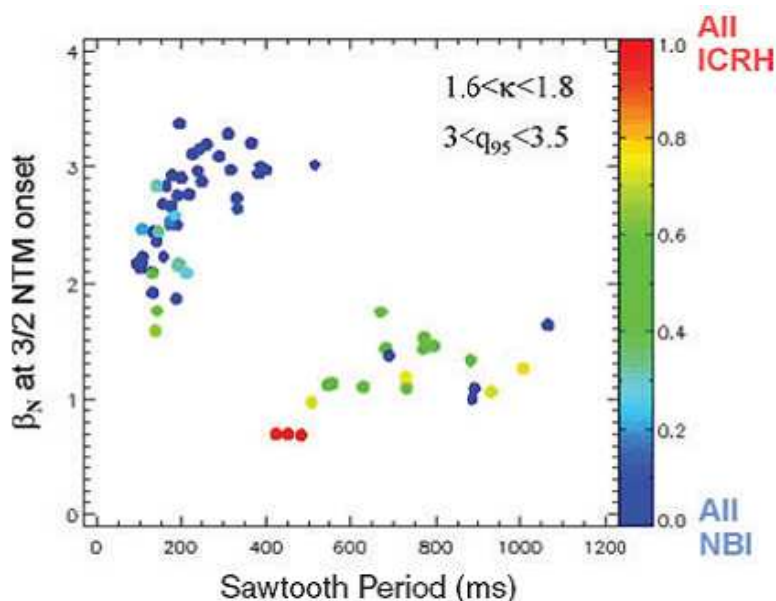


Figure 5. Dependence of NTM onset β_N with sawtooth period for NBI-only and core deposition ICRH discharges for standard shape H-mode plasmas in JET (right-hand side colour scale indicates degree of ICRH : NBI power) Reproduced with permission from *Buttery et al* [14].

small amplitude sawtooth crashes. At the same time, the sawtooth period must be longer than the slowing down time of the fusion α particles in burning plasmas, or else the energetic α particles could be lost from the plasma core before they transfer their energy to the thermal plasma to ensure continuing fusion reactions.

In recent years there has been considerable progress in both the theoretical understanding of sawtooth control and the experimental implementation of control schemes. In section 2, recent developments in the theoretical understanding of the physics of sawtooth stability are discussed. Such improved understanding, for instance, concerning the role of passing energetic ions, has significant implications for sawtooth control actuators. Models that predict when a sawtooth crash will occur are also outlined. Sawtooth control achieved by locally perturbing the current profile is discussed in section 3. By changing the magnetic shear near the $q = 1$ surface, the sawtooth period can be significantly influenced. Recent results exhibiting destabilisation of sawteeth by steerable electron cyclotron resonance heating (ECRH) are presented, including real-time feedback schemes and electron cyclotron current drive (ECCD) control in the presence of energetic ions in the plasma core. These results justified the inclusion of ECCD for sawtooth control in the ITER design [8].

Sawtooth control can also be achieved by modifying the fast particle distribution. In section 4, sawtooth behaviour in plasmas heated by neutral beam injection (NBI) is examined. Differences in the sawtooth period in plasmas with NBI either in the same direction as the plasma current or opposing it have provided great insight into the physical mechanisms that underlie sawtooth stability. Furthermore, the injection

of NBI outside the $q = 1$ surface is shown to have an application as a sawtooth control tool due to changes in the spatial gradient of the fast ion population. The increased understanding of kinetic effects on sawtooth stability arising from these NBI experiments also has implications for our understanding of sawtooth control achieved with ion cyclotron resonance heating (ICRH). The significant stabilisation of sawteeth in plasmas heated with ICRH first highlighted the important role played by fast ions. Since then, ICRH has also been used to destabilise sawteeth, as described in section 5 through a combination of current drive and kinetic effects. Finally, the implications of these recent developments in sawtooth control techniques for ITER are discussed in section 6.

2. The Physics of Sawtooth Stability

Since a sawtooth crash is usually accompanied by an $m = n = 1$ kink displacement [32], much of the work to try to explain the sawtooth phenomena has centred on the stability of the 1/1 internal kink mode. The kink mode is so called because it leads to a kinking of the magnetic surfaces. In regions of high current there is a strong poloidal magnetic field induced by the current. Should the plasma then experience a perturbation, the strong poloidal magnetic field will reinforce the instability and push the plasma further out, extending the “kinking” effect [2]. The potential energy of the perturbation can be derived for a circular, large-aspect ratio tokamak ($\epsilon = a/R \ll 1$) as

$$\delta W = \frac{\pi^2 B_\phi^2}{\mu_0 R} \int \left[\left(r \frac{d\xi_r}{dr} \right)^2 + (m^2 - 1) \xi_r^2 \right] \left(\frac{n}{m} - \frac{1}{q} \right)^2 r dr + O(\xi^2) \quad (1)$$

Equation (1) is minimised when $m = n = 1$ and $d\xi/dr = 0$. A rigid displacement, $\xi = \text{constant}$ is not permitted since $\xi_a = 0$ for internal modes. However, a top-hat displacement which is rigid within the $q = 1$ surface and zero outside is an allowed solution which minimises the potential energy of the mode. Such a solution means that the first term in equation (1) is identically zero and the stability of the mode is determined by higher order ξ^2 terms related to the pressure gradient. However, sawtooth stability in tokamak plasmas is not determined solely by the fluid drive of the 1/1 internal kink mode; its dynamics are significantly affected by the presence of energetic particles, by sheared flows, by pressure anisotropy, by diamagnetic effects, by complex nonlinear reconnection physics and local effects in the inertial layer around the $q = 1$ surface (ie the discontinuity in the eigenfunction). All of these effects have implications for the actuators available to control sawtooth oscillations. Hereafter follows a brief review of recent theoretical developments concerning the stability of the internal kink mode which are pertinent to effective control schemes.

2.1. Effect of Energetic Particles

In 1986, high power ion cyclotron resonance heating (ICRH) experiments were conducted in JET, in which the sawtooth instability was suppressed for many seconds [33]. Further

experiments using ICRH showed that long sawtooth quiescent periods were terminated abruptly by a sawtooth collapse that followed the switch off of the ICRH with a time delay of ~ 80 ms (approximately the same as the slowing down time of the hot ICRH ions) [34]. This suggested that the ICRH fast ions provided a stabilising influence upon the sawteeth. The stabilising effect of fast ions was later confirmed using NBI [10], though only in a few specialised cases could quiescent periods be achieved which were comparable with those in ICRH heated plasmas. It was also shown that fusion-born α particles produced a strongly stabilising effect on sawteeth [35].

After this experimental evidence that sawteeth could be strongly stabilised by the presence of an energetic particle population, there followed a significant theoretical effort to explain this phenomenon. Much of this work followed the principles developed by Chen *et al* [36] to explain the fishbone instability [37] – another $m = n = 1$ internal kink instability that is driven by the presence of energetic particles. The dispersion relation, developed most notably by White *et al* [38–40], gives

$$i\sqrt{\omega(\omega - \omega_{*i})} \sim \delta W_{MHD} + \delta W_{hf} + \delta W_{hk}^t \quad (2)$$

where δW_{hf} and δW_{hk}^t are the fluid and kinetic components respectively. Only the trapped fast particles were considered at first. This equation was found to have two branches: The first, when $\Re(\omega) \sim \langle \omega_{dh} \rangle$ and $\langle \omega_{dh} \rangle$ is the bounce-averaged magnetic drift frequency of the hot ions, characterises the fishbone instability [36]. The second, when $\Re(\omega) < \langle \omega_{dh} \rangle$, is responsible for sawteeth. The trapped energetic ions were predicted to provide significant sawtooth stabilisation providing the lower frequency branch satisfied $\Re(\omega) \ll \langle \omega_{dh} \rangle$.

Not only the α particles and the ICRH and NBI fast ions affect the stability of the kink mode. Kruskal and Oberman [41] showed that the plasma thermal ions can also stabilise core MHD instabilities. Later the effects of thermal ions were considered using the energy principle including the guiding centre motion of the energetic particles [42], and again, were found to have a stabilising influence upon the kink mode [43, 44]. Kruskal-Oberman theory applies only to collisionless thermal trapped ions when the characteristic mode frequency exceeds the thermal ion diamagnetic frequency, $\omega > \omega_{*i}$. Typically, $\delta W_{KO} > \omega_{*i}\tau_A$, so the contribution of these thermal ions is non-negligible. The change in the potential energy of the $n/m = 1/1$ internal kink mode due to the trapped thermal ions is given by

$$\delta W_{KO} = \frac{1}{2} \int \boldsymbol{\xi}_\perp \cdot (\nabla \cdot \delta P_{ki}) d\mathbf{r} \quad (3)$$

where δP_{ki} is the perturbed thermal ion pressure tensor, $\delta P_{ki} = -\boldsymbol{\xi}_\perp \cdot \nabla P_i$. This term is equivalent to the compressibility term in ideal MHD. When the kink instability grows, the orbiting ions are compressed. The passing ions are able to squirt along the compressed field lines, but the trapped ions result in $\nabla \cdot \boldsymbol{\xi}_\perp \neq 0$, which is stabilising. It is worth noting that the limit for applicability of the Kruskal-Oberman term ($\omega \gg \omega_{*i}$) is never satisfied since the most unstable mode is either the drift tearing mode ($\omega \sim \omega_{*e}(r_1)$), the resistive kink mode ($\omega \sim 0$) or the ion drift mode ($\omega \sim \omega_{*i}$).

2.1.1. Trapped Energetic Ions The mechanism for the stabilisation of the low-frequency MHD perturbations by trapped fast ions is a result of the conservation of the third adiabatic invariant [45, 46]. Porcelli proposed that in a tokamak equilibrium, this third adiabatic invariant of motion [47], Φ_{ad} , is equivalent to the flux of the poloidal magnetic field through the area defined by the toroidal precession of the trapped particle orbit centres. In order for Φ_{ad} to be conserved, the time it takes a trapped ion to complete a toroidal orbit must be short compared to the timescale of the mode, $2\pi/\omega$. The fast ions can be viewed as a distribution of current loops (in equilibrium with the fast particle pressure) [45]. The current in each of these loops is analogous to the precessional drift frequency of the trapped particle. These loops have a poloidal flux through the area which they enclose. If the plasma experiences an $n/m = 1/1$ displacement, the poloidal flux through this area would change.

By employing the generalised energy principle, the change in the potential energy of the kink mode due to the energetic trapped ions can be calculated. The fast ion distribution function is typically separated into an equilibrium component, $f_0(\mathcal{E}^0, \mathcal{P}_\phi^0, \mu)$, and two perturbed components, $\delta f_h = \delta f_{hk} + \delta f_{hf}$, a non-adiabatic (kinetic) and an adiabatic (fluid) part respectively. Here, a particle is said to behave adiabatically if its characteristic motion around a closed orbit is much faster than the temporal and spatial scales associated with a perturbation (ie the perturbation appears as a static modification of the equilibrium). The particle energy ($\mathcal{E}^0 = Mv^2/2$), the canonical momentum ($\mathcal{P}_\phi^0 = MB_\phi v_\parallel/B - e\psi_p$) and the magnetic moment ($\mu = Mv_\perp^2/2B$) are the unperturbed constants of motion. Analytic theory developed for large aspect ratio circular plasmas [48] can be used to express these contributions to the perturbed distribution function as

$$\delta f_{hk} = \sum_{l=-\infty}^{\infty} \frac{\tilde{\omega} - \Delta\Omega - n\omega_{*h}}{\tilde{\omega} - \Delta\Omega - n\langle\dot{\phi}\rangle + l\omega_b} \frac{\partial f_h}{\partial \mathcal{E}^0} e^{-i(\omega + l\omega_b + n\langle\dot{\phi}\rangle)t} \quad (4)$$

$$\times \left\langle \left(v_\parallel^2 + \frac{v_\perp^2}{2} \right) \boldsymbol{\kappa} \cdot \boldsymbol{\xi}_\perp e^{i(\omega + l\omega_b + n\langle\dot{\phi}\rangle)t} \right\rangle$$

$$\delta f_{hf} = -\frac{Ze}{M_h} \boldsymbol{\xi} \cdot \nabla \psi_p \frac{\partial f_h}{\partial \mathcal{P}_\phi^0} \quad (5)$$

respectively, where $\omega_{*h} = (\partial f_h / \partial \mathcal{P}_\phi^0) / (\partial f_h / \partial \mathcal{E}^0)$ is the hot ion diamagnetic frequency, $\omega_b = 2\pi/\tau_b$, τ_b is the poloidal orbit transit time, M_h is the fast ion mass, the dots represent the derivative with respect to time, $\Delta\Omega = \Omega_E(r) - \Omega_E(r_1)$ is the sheared toroidal flow, $\tilde{\omega}$ is the Doppler shifted mode frequency, l is the poloidal quantum number and $\langle \dots \rangle$ defines an average. Given δf , the hot particle contribution to the potential energy of the $n = 1$ internal kink mode is then calculated as [45, 49, 50]

$$\delta W_h = \frac{1}{2} \int d\Gamma (Mv_\parallel^2 + \mu B) \delta f \sum_m \boldsymbol{\kappa} \cdot \boldsymbol{\xi}^{(m)*}(r, t) e^{-i(n\phi - m\theta)} \quad (6)$$

where θ is the poloidal angle, $\boldsymbol{\kappa} = \mathbf{b} \cdot \nabla \mathbf{b}$ is the magnetic curvature vector and $\mathbf{b} = \mathbf{B}/B$.

It had been observed that NBI did not stabilise sawteeth as effectively as ICRH [51]. This was thought to be because NBI minority ions are far less energetic than ICRH

ions, meaning that they were less likely to satisfy the condition for conservation of Φ_{ad} : $\Re(\omega) \ll \langle \omega_{ah} \rangle$. However, NBI also leads to greater plasma rotation, flow shear and anisotropy than achieved with ICRH. These important effects have subsequently been included in the model for kinetic stabilisation of the internal kink mode by trapped ions [48, 52, 53].

2.1.2. Passing Energetic Ions For many years it has been known that trapped energetic particles result in strong stabilisation of sawteeth. However, passing fast ions can also significantly influence sawtooth behaviour. For highly energetic ions, the radial drift motion becomes comparable to the radial extent of the kink mode. In this regime, the kinetic contribution to the mode's potential energy associated with the passing fast ions (together with a non-convective contribution to the fluid part of δW) becomes increasingly important.

Previous investigations of the effects of passing ions on the high-frequency fishbone branch of the $n = 1$ kink mode suggested that the circulating ions would not affect mode stability in the limit $\omega \rightarrow 0$ [56]. However, when the passing fast ion population is asymmetric in velocity space, there is an important finite orbit contribution to the mode stability. Recent studies including the non-adiabatic effects find that the passing ions can stabilise the kink mode [57]. Later the adiabatic effects were also included, and Graves found that the non-adiabatic contribution was counteracted by the adiabatic terms, but that an additional adiabatic contribution survives which can significantly affect the mode stability [58]. This strong contribution of the circulating particles comes from the ions close to the trapped-passing boundary where their orbit widths, Δ_b are large, $\delta W_h^p \sim \Delta_b$. The non-adiabatic passing ion effects arise due to the gradient ∇f_h integrated over the $q = 1$ radius, whereas the adiabatic terms arise due to fast ions which intersect the $q = 1$ surface, and so depend only on $\partial P_h / \partial r|_{r_1}$. Whilst only ideal stability was first considered in this model, it has also been shown that including resistivity only slightly modifies the stability boundary and the instability is still driven by the asymmetric passing ions [59]. The effect of passing ions is enhanced for large effective orbit widths [60], which is to say, for highly energetic ions (like ICRH or N-NBI in ITER) or for a population with a large fraction of barely passing ions (like NBI in JET). Passing fast ions can destabilise the internal kink mode when they are co-passing and the fast ion distribution has a positive gradient across $q = 1$, or when they are counter-passing, but the deposition is peaked outside the $q = 1$ surface. This mechanism is described in detail in references [58] and [61] with an overview of fast ion effects in reference [60].

2.2. Effect of Toroidal Rotation

2.3. Equilibrium Mass Flow of the Order of the Sound Speed

As well as giving rise to a population of energetic particles, NBI also results in a toroidal rotation of the plasma, sometimes at speeds approaching the ion thermal speed [63]. When this toroidal rotation reaches a significant fraction of the sound speed, the

centrifugal effects can also affect kink mode stability. Waelbroeck [64] first considered the gyroscopic stabilisation of the internal kink mode arising from centrifugal effects in 1996. Later Wahlberg and Bondeson [65] revisited the problem and emphasised the role of density gradients which are established on flux surfaces due to toroidal rotation. The establishment of such density gradients are also found to be stabilising to the quasi-interchange mode [66]. Subsequent modelling of the effects of sheared toroidal flows on MHD modes found that rotation approaching the ion sound speed could completely stabilise the ideal $n = 1$ kink mode [67, 68], implying that the longer quiescent periods observed in NBI heated plasmas were not only due to the fast ions, but also the ancillary stabilising effect arising from the beam-driven plasma rotation. Recent analytic theory has shown that the stabilisation attributed to gyroscopic effects in [64] and density stratification in [65] can be explained mathematically as a result of the finite continuum frequency in the $q = 1$ layer. The geodesic acoustic mode (GAM) induced by plasma rotation exists solely due to the nonuniform plasma density created by the centrifugal force and coupling to this mode results in a stabilising effect on the $n = 1$ internal kink mode. Furthermore, modelling the stability of the internal kink mode is highly sensitive to the consistent treatment of equilibrium flows [69] and the precise density and rotation profiles [70].

2.4. Flows of the Order of the Diamagnetic Velocity

Even for slow rotation speeds of the order ω_{*i} , the *shear* of the rotation profile can affect the stabilisation arising from the trapped ions. Theoretically it is found that the kinetic stability of the kink mode depends sensitively upon the sheared toroidal plasma rotation. Conservation of the third adiabatic invariant, Φ_{ad} is only obtained [52] when $\langle \omega_{dh} \rangle + \Delta\Omega - \tilde{\omega} \gg 0$. Since this condition is more readily satisfied for co-rotation ($\Delta\Omega > 0$), plasmas with co- I_P velocity shear support more effective stabilisation of the kink mode, because particles with low energy are able to provide a positive contribution through equation (4). Conversely, the stabilising effect is diminished in counter-rotating plasmas ($\Delta\Omega < 0$) since Φ_{ad} -conservation is inhibited, and the stabilising contribution can only come from the less numerous higher energy ions. At very large flows, δW_{hk} tends to an asymptotic limit, since $\Delta\Omega$ dominates both numerator and denominator in equation (4). The plasma flow will only influence mode stability when $|\Delta\Omega| \sim \omega_{*i}$. As such it is the collisionless response of the low energy ions that is significantly modified by rotation. It is predicted [54, 55] that ITER plasmas will rotate at $v_\phi < 0.02v_A$ ($\omega_\phi \sim 2\omega_{*i}$). This low rotation means that the condition for sheared flow to influence stability is unlikely to be met in ITER.

2.5. Sawtooth Crash Trigger Modelling

The fundamental trigger of the sawtooth crash is the onset of an $m = n = 1$ mode. The dynamics of this instability are constrained by many factors including not only the macroscopic drive from ideal MHD, but collisionless kinetic effects related to high

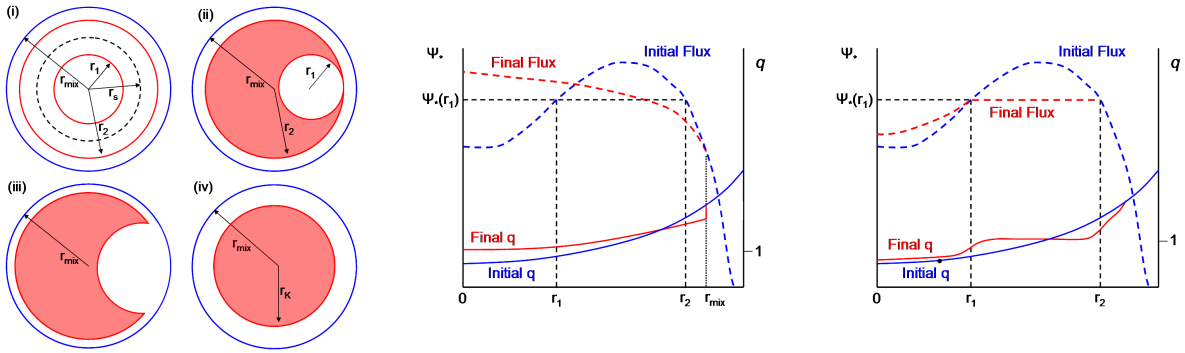


Figure 6. (a) The Kadomtsev model of the sawtooth crash, showing (i) magnetic flux surfaces before reconnection with r_1 and r_2 as surfaces with the same helical flux which reconnect in (ii). The island separatrix deforms into a broader crescent in (iii) before complete reconnection occurs with the magnetic axis reconnecting with r_{mix} in (iv); (b) The safety factor and helical flux profiles before and after complete reconnection; and (c) partial reconnection.

energy particles described in section 2.1 and rotation effects described in section 2.2, as well as non-ideal effects localised in the narrow layer around $q = 1$. Finite electrical resistivity, electron compressibility, diamagnetic effects, finite orbit width effects [71, 72], semi-collisional electron physics [71, 73] and low collision-frequency kinetic theory which implies neoclassical effects can also play a role in determining the stability threshold for a sawtooth crash. Whilst there have been notable advances in all of these aspects of layer theory, as yet, no stability threshold incorporates all the requisite physics. The phenomenology of sawtooth oscillations and their theoretical interpretation is reviewed in references [1], [74] and [75]. A very brief recapitulation on the understanding of the sawtooth crash is given here, with a view to how this influences the ability of a given actuator to affect when a crash will occur.

The first ideal MHD description of the ideal internal kink mode in a cylindrical plasma [76] was found to be inadequate to describe the sawtooth phenomenon without incorporating resistive effects. Bussac et al [77] showed that the ideal internal kink was stable at sufficiently low β_p in toroidal plasmas with $q < 1$, though the resistive kink remained unstable [78]. Soon after these developments in the theory of the internal kink mode, Kadomtsev proposed a nonlinear complete reconnection model [79] to describe the sawtooth evolution. This model is based upon two assumptions, namely that magnetic surfaces of equal helical flux reconnect, and that the toroidal flux is conserved during this reconnection. When the safety factor goes below unity, the resistive or ideal internal kink mode leads to a displacement of the central region of the plasma ($q < 1$), which in turn results in the crowding of flux surfaces on one side and formation of a magnetic X-point. Subsequently, an $m = 1$ magnetic island grows such that each pair of surfaces with equal helical flux touch and reconnection occurs. An intermediate state is formed, with a circular hot core partially surrounded by a cooler island [74, 80]. This is followed by the expulsion of the hot core and a new cylindrically symmetric equilibrium is established. This process is illustrated in figures 6(a) and 6(b). Kadomtsev gave an estimate for the

reconnection time, $\tau_K \approx (\pi R r_1^2 / \eta c^2 v_A)^{1/2}$ where r_1 is the radius of the $q = 1$ surface, η is the resistivity, $v_A = B_0 / \sqrt{\mu_0 \rho_0}$ is the Alfvén speed and ρ_0 is the equilibrium mass density. In order to re-establish an equilibrium with $q > 1$ for resistive kink stability, the $m = 1$ island was assumed to grow until it filled the entire volume inside $q = 1$ – referred to as complete reconnection. However, there soon followed vitiation of the Kadomtsev model when detailed measurements of the soft X-ray emission during a sawtooth cycle suggested that the relatively slow $m = 1$ reconnection process was suddenly interrupted by some secondary instability whilst the magnetic island was still of only modest size [81] and q -profile measurements indicated that q remained below unity after the thermal crash [82–85], in contradiction with Kadomtsev’s full reconnection concept. Finally, the advent of large tokamaks provided further evidence conflicting with Kadomtsev’s model, since the reconnection timescale is too slow to explain the observed crash times [86].

These advances in the experimental diagnosis of the sawtooth cycle led to the proposal of many alternative crash trigger models, including resistive two-fluid MHD [87, 88], collisionless kinetic effects [41, 42, 89], accelerated complete reconnection due to nonlinear collisionless effects [90], magnetic stochastization which led to enhanced perpendicular transport [91], chaos [92], the quasi-interchange model [93] and triggering of secondary instabilities [94–97]. Each of these models has had proponents and experimental support over the years. However, recent advances in imaging electron temperature fluctuations with high temporal and spatial resolution [5, 6] have given new information about the nature of the sawtooth crash event. The experimental observations of Park *et al* [6] suggest that the global stochasticity of the magnetic field [91] is not the dominant crash mechanism since the heat transport exhibits well organised, collective behaviour. Furthermore, triggering of a ballooning instability [95, 96] is also unlikely to cause the crash phase, because, although the localised pressure bulges seen experimentally are consistent with ballooning modes, they are often observed to be localised in a region of good curvature, which violates ballooning theory. These new observations do not, however, conflict with the most widely-accepted crash trigger model, the partial reconnection model [22, 94].

In the partial reconnection model, the magnetic surfaces begin to undergo reconnection, just as in the Kadomtsev model [79]. However, when the magnetic island reaches a critical width, a relaxation occurs, with the core region and critical island region undergoing different relaxation processes. The inner core Taylor relaxes, as proposed in reference [94], whilst the reconstructed surfaces in the island region have the same helical flux, as in full reconnection. This partial reconnection [98] results in the formation of two current sheets, which diffuse rapidly during the next sawtooth ramp, as illustrated in figure 6(c).

The fundamental trigger of the sawtooth crash remains the onset of an $m = n = 1$ mode, although the dynamics of this instability are constrained by many factors including not only the macroscopic drive from ideal MHD, but collisionless kinetic effects related to high energy particles [45, 48, 58] and thermal particles [41], as well as non-ideal effects localised in the narrow layer around $q = 1$. A heuristic model predicts that a

sawtooth crash will occur when one of the following criteria is met [22, 99]:

$$-\delta\hat{W}_{core} > c_h\omega_{dh}\tau_A \quad (7)$$

$$-\delta\hat{W} > \frac{1}{2}\omega_{*i}\tau_A \quad (8)$$

$$-c_\rho\hat{\rho} < -\delta\hat{W} < \frac{1}{2}\omega_{*i}\tau_A \quad \text{and} \quad \gamma_{eff} > \frac{1}{c_*}\sqrt{\omega_{*i}\omega_{*e}} \quad (9)$$

where ω_{dh} is the magnetic drift frequency of the hot ions, $\tau_A = \sqrt{3R}/v_A$ is the Alfvén time, c_h , c_ρ and c_* are normalisation coefficients of the order of unity, γ_{eff} is the effective growth rate of the resistive internal kink mode [99] and $\hat{\rho} = \rho_i/r_1$. The change in the kink mode potential energy is defined such that $\delta\hat{W}_{core} = \delta\hat{W}_{MHD} + \delta\hat{W}_{KO}$ and $\delta\hat{W} = \delta\hat{W}_{core} + \delta\hat{W}_h$ where $\delta\hat{W}_{KO}$ is the change in the mode energy due to the collisionless thermal ions [41], $\delta\hat{W}_h$ is the change in energy due to the fast ions and $\delta\hat{W}_{MHD}$ is the ideal fluid mode drive [77, 100]. The potential energy is normalised such that $\delta\hat{W} \equiv 4\delta W/(s_1\xi_0^2\epsilon_1^2RB^2)$. The second part of equation (9) can be recast in terms of a critical magnetic shear determined by the pressure gradient, $s_1 > s_{crit}(\omega_{*i})$, which means that the concurrent criteria in equation (9) can be rewritten as:

$$s_1 > \max\left(s_{crit} = \frac{4\delta W}{\xi_0^2\epsilon_1^2RB^2c_\rho\hat{\rho}}, s_{crit}(\omega_{*i})\right) \quad (10)$$

It is found that in auxiliary heated plasmas, the most relevant criterion from equations 7-10 for determining the onset of the sawtooth crash is equation 10. Consequently, long period sawteeth can be destabilised (ie a crash can be triggered) by enhancing s_1 (through localised current drive), or through δW reduction or reversal. Data from TFTR plasmas [101] showed that sawteeth occurred when the magnetic shear at $q = 1$ exceeded a critical value given by collisionless theory [102] strongly supporting the enhancement of the magnetic shear as a sawtooth control actuator. Despite its heuristic formulation and the fact that the model is based solely on linear stability thresholds, the linear model proposed by Porcelli *et al* [22] has had notable success when applied to simulate the observed sawtooth period in tokamak plasmas [98, 103–105].

2.6. Sawtooth Control Actuators

Sawtooth control refers to the ability of an actuator (be it a heating and/or current drive system or plasma shaping control) to alter the sawtooth period. The two approaches to sawtooth control are to (i) either eliminate or delay the sawtooth crash for as long as possible (stabilisation) or (ii) decrease the sawtooth period to reduce the likelihood of triggering other MHD instabilities (destabilisation). Sawtooth control can be achieved by tailoring the distribution of energetic ions; by changing the radial profiles of the plasma current density and pressure, notably their local gradients near the $q = 1$ surface; by rotating the plasma, or changing the rotation shear local to the $q = 1$ surface; by shaping the plasma; or by heating the electrons inside the $q = 1$ surface. The primary

actuators to achieve these perturbations are electron cyclotron current drive (ECCD), ion cyclotron resonance heating (ICRH) and neutral beam injection (NBI).

The highly localised perturbations to the current density profile achievable with ECCD have been employed to significantly alter sawtooth behaviour on a number of devices. By driving current just inside the $q = 1$ surface, the magnetic shear at $q = 1$ can be increased, and thus result in more frequent sawtooth crashes. This can be understood by considering equation 10 where the linear crash criterion is satisfied when the magnetic shear at $q = 1$ is sufficiently large. ECCD has been included as the primary sawtooth control actuator in the ITER design [8] due to both the highly localised current density that can be achieved when compared to ICCD for instance, and because of the ability to provide real time control of the current drive location by changing the launcher angle of the injected EC beam by using steerable mirrors. This means that the deposition can be moved as the q -profile evolves due to current penetration, which is much easier than changing ICRH frequency or NBI deposition location. However, some concerns remain regarding the ability of ECCD to destabilise sawteeth in the presence of a significant population of fast particles in the core, as will be the case in ITER. This concern is exemplified by equation 9 where the left hand side, ρ/r_1 , will be very small since ρ is small and r_1 is predicted to extend towards mid-radius in ITER baseline scenario, and the right hand side is likely to have a large δW_h in the numerator due to the presence of the α particles.

Fortunately, other actuators can influence the magnitude of δW directly. Neutral beam injection affects the change in the potential energy of the internal kink mode in two ways: Firstly, it gives rise to a significant population of energetic particles in the plasma. The predominantly passing fast ions can destabilise the sawteeth when they are injected in the same direction as the plasma current and outside the $q = 1$ surface, or opposite to the plasma current and inside $q = 1$. Secondly, NBI also results in a torque on the plasma, and significant toroidal rotation can stabilise the internal kink mode too. However, due to the rather broad $q = 1$ surface expected in ITER [8], the N-NBI energetic ions are likely to be born inside $q = 1$, even when injected at the most tangential angle of injection [24], meaning that (at least for co-NBI) they will always be strongly stabilising and cannot be used to shorten the sawtooth period. That said, if the sawtooth period can be kept short, r_1 will also be small, enhancing the ability of off-axis NBI to affect the sawtooth behaviour.

Conversely, ion cyclotron resonance heating can give rise to a population of energetic particles outside $q = 1$ in ITER. Initial studies of the effects of ICRH on sawtooth behaviour concluded that the (de)stabilisation achieved arose due to the driven current changing the magnetic shear local to $q = 1$. However, recent studies have shown that ICRH sawtooth control persists in plasmas where the driven current is negligible, highlighting that the ICRH destabilisation mechanism also includes strong kinetic effects. For instance, it has been shown [61] that the fast ion population born due to off-axis ^3He minority RF-heating scenarios, like the operating scenario proposed for ITER, can give rise to sawtooth destabilisation, even in the presence of core fast ions.

Detailed modelling of the scope and power requirements for the various sawtooth control actuators in ITER is in progress.

3. Current Drive Schemes

When electron cyclotron resonance heating (ECRH) is applied to the plasma, a change in the local current density occurs due to the change in the temperature, and subsequent change in the conductivity. This changes the magnetic shear at $q = 1$, s_1 , which increases the likelihood of a sawtooth crash, as seen in equation 10. Furthermore, by adding a toroidal component to the wave vector of the launched EC waves, an ancillary electron cyclotron driven current results either parallel (co-ECCD) or anti-parallel (counter-ECCD) to the Ohmic current, enhancing the potential to change s_1 . The control of sawteeth by modification of the local current density has now been demonstrated in a number of tokamaks, and consequently has been included in the design of the sawtooth control system for ITER.

Early experiments to assess the capability of current drive schemes for affecting sawtooth behaviour focussed on lengthening the sawtooth period [7, 106–109]. Indeed, it was shown that with careful placement of the deposition location of the ECCD, sawteeth could be stabilised for the entire gyrotron pulse length on WT-3 (0.03s) [110], TEXTOR (0.2s) [111], JT-60U (1.5s) [112] and ASDEX Upgrade (2.0s) [113]. Soon after the observation that driving local current could lengthen the sawtooth period, sawtooth destabilisation was also achieved [114]. ECCD has also been shown to be more effective than ECH (here defined as when the beam injection angle is perpendicular to the magnetic axis) [119, 120], although electron heating does have an indirect effect on the current by changing the local resistivity profile. In all cases, strong changes in the sawtooth period are found for very small changes in the deposition location (of the order of the deposition width, typically a few cm) with respect to the location of the $q = 1$ surface, see for example reference [107]. It is this strong localisation of the driven current which makes ECCD a robust sawtooth control actuator, even when the driven current is as little as 1% of the Ohmic current [121–123]. Provided that the magnetic shear at $q = 1$ is altered sufficiently to overcome the stabilising terms in δW in equation 9, then the ECCD can affect sawtooth behaviour even when the driven current is small. ECCD has been shown to be a successful sawtooth control actuator in a number of devices including ASDEX Upgrade [119, 124–126], TCV [104, 121, 127, 128], JT-60U [112, 129], DIII-D [120], TEXTOR [17, 111], Tore Supra [130, 142], FTU [131] and WT-3 [132]. Sawtooth control can be enhanced by maximising the local ECCD current density rather than the total driven current at the expense of narrowing the deposition width [124].

The first ECCD destabilisation experiments performed a sweep of the deposition location across the $q = 1$ surface by ramping the magnetic field. It was found that the sawtooth period was highly sensitive to the location of the deposition with respect to the sawtooth inversion radius [108, 109, 134]. In accordance with equation 10, increasing the

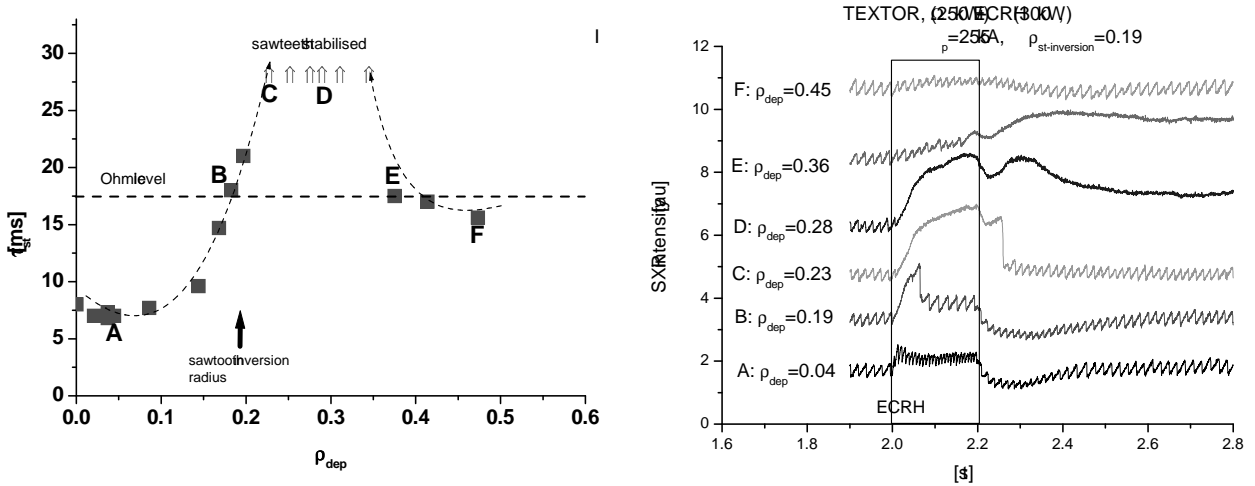


Figure 7. (left) The sawtooth period as a function of ECRH deposition location in TEXTOR compared to the inversion radius. The letters refer to discharges shown in the (right) figure. Reproduced with permission from *Westerhof et al* [111].

current just inside $q = 1$ increases s_1 and so destabilises the sawteeth, whilst co-ECCD localised just outside $q = 1$ decreases s_1 and so stabilises the sawteeth. Conversely, counter-ECCD just inside $q = 1$ results in stabilisation and just outside $q = 1$ gives rise to destabilisation [104,119,122,123]. Figure 7 shows the sawtooth period with respect to the deposition location of the ECCD in TEXTOR [111]. It is evident that when the co-ECCD is deposited just inside the inversion radius, the sawtooth period can be shortened to a level below Ohmic sawtooth periods, but that as the co-ECCD moves to just outside $q = 1$ the sawteeth are completely stabilised. Such behaviour is demonstrated in many other machines as well, for example in references [104,108,109,119,134]. ECCD power scans have also shown that as the driven current is increased, the effect on the sawtooth behaviour can be enhanced. Figure 8 shows the sawtooth behaviour as the co-ECCD power is increased in ASDEX Upgrade when the deposition location is just inside the $q = 1$ surface [119]. It is clear that the sawtooth period decreases with increasing co-ECCD power, and consequently, EC driven current. Similar power ramps have been shown to increase the sawtooth period when the deposition is located outside $q = 1$ [119,135]. Finally, it is worth noting that the control of sawteeth for NTM prevention using ECCD has been demonstrated directly on ASDEX Upgrade. Reference [125] shows that NTMs are avoided at high β_N by complete suppression of the sawteeth using co-ECCD just outside the $q = 1$ surface. Concomitant with the end of the gyrotron pulse, a sawtooth crash occurred and an NTM was triggered, resulting in a substantial degradation of the plasma performance.

In parallel to the extensive experimental evidence that applying ECCD could strongly affect the sawtooth period, complementary numerical modelling gave rise to an enhanced understanding of the physical mechanisms which underlie this actuator. In order to model the sawtooth period, the transport during the ramp phase must be accurately modelled in order to assess when the linear crash criteria of equations

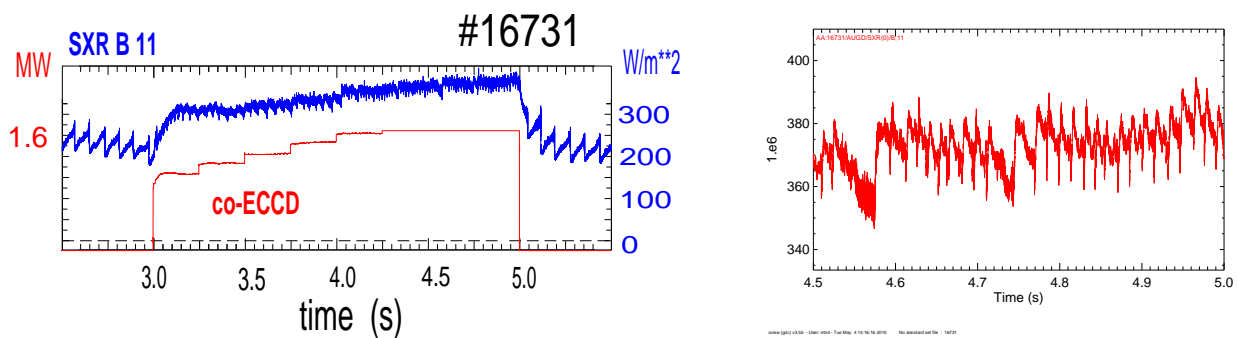


Figure 8. (left) The sawtooth behaviour in ASDEX Upgrade as the co-ECCD power is increased with a deposition inside $q = 1$. As the gyrotron power is ramped up, the sawtooth period decreases. (right) A blown-up image showing the fine-scale sawtooth behaviour. *Mueck et al* “Sawtooth control experiments on ASDEX Upgrade” *Plasma Phys. Control. Fusion* **47** 1633 (2005) [119] published by Institute of Physics Publishing.

7 to 9 are met. Discharges with ECH, and co- and counter-ECCD in TCV have been modelled using the PRETOR-ST code [104, 121] – a transport code including a model for determining when a sawtooth crash will occur based on the linear stability thresholds given in [22]. The modelling shows that whilst co- and counter-current drive have opposite effects, the anti-symmetry is broken by ancillary localised heating. Since the heating acts like co-ECCD, the most efficient destabilisation occurs with co-ECCD and ECH just inside the $q = 1$ surface, whilst the most efficient stabilisation occurs with co-CD and ECH outside $q = 1$ [104]. The PRETOR-ST calculations indicated that the variation in the rate of change of the magnetic shear was the predominant physical mechanism in determining the sawtooth period. Figure 9 shows the sawtooth period in TCV as observed experimentally and as predicted numerically by transport modelling when one ECH beam oriented just outside $q = 1$ to stabilise the sawteeth and a second beam swept outwards across the inversion radius. The simulations accurately predict the sawtooth period and behaviour during the ECCD sweep, despite being based upon a full reconnection model. Similar ASTRA [136] modelling helped to explain the difference between co- and counter-ECCD on ASDEX Upgrade and once again identified the modification of the magnetic shear as the leading physical mechanism for affecting the sawtooth behaviour [119]. A simplified model of the poloidal field evolution has been benchmarked against both ASTRA modelling and TEXTOR experimental results in order to provide insight into the non-inductive current drive requirements for sawtooth control [137]. Assuming a factor of two change in the magnetic shear is necessary to influence the sawtooth behaviour (though the effect of fast ions is largely neglected in the assumption), it was found that the requisite non-inductively driven current is given by $I_{cd} \geq 2(\Delta r/r_1)^2 I_{q=1}$ where Δr is the Gaussian width of the ECCD profile and $I_{q=1}$ is the total current encompassed by the $q = 1$ surface. A more accurate assessment of non-inductive current drive requirements in ITER was made by Zucca *et al* [138, 139], as discussed in section 6.

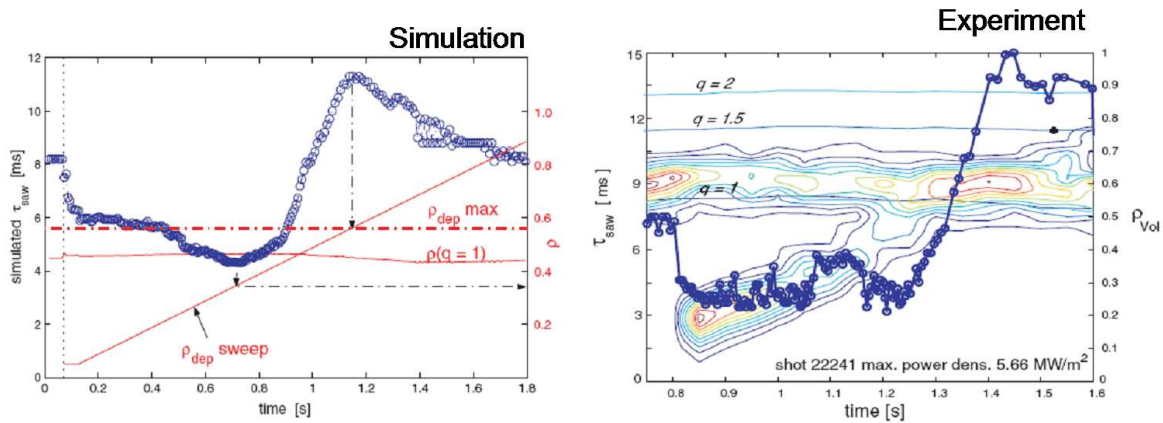


Figure 9. (left) Predictions of the sawtooth period from the PRETOR-ST code and (right) the measured sawtooth period in TCV with ECH beams directed on-axis to stabilise the sawteeth and an ancillary ECH beam is swept across the inversion radius. The contours in the right figure indicate the location of the heat deposition relative to the minor radius, r . Reproduced with permission from *Angioni et al* [104].

By sweeping the magnetic field or plasma position to alter the deposition location of the ECCD with respect to the $q = 1$ surface, the optimum settings for sawtooth control can be ascertained. However, whilst the experiments performed using magnetic field ramps to sweep the deposition location of the ECCD have significantly improved our understanding of the control mechanisms, the major advantage of current drive schemes is that ECCD provides a simple external actuator in a feedback-control loop through the angle of inclination of the launcher mirrors. Consequently, recent studies have focussed on real-time control of the deposition location in order to obtain requested sawtooth periods. Indeed, the uncertainties in the control parameters (such as the launcher aiming and ray-tracing prediction for the resultant driven current) and the plasma equilibrium parameters (such as the $q = 1$ location and plasma position), coupled with the strong sensitivity of the sawtooth period to the deposition location relative to $q = 1$, mean that real-time feedback is a necessity for robust control reliant upon current drive schemes. TCV has demonstrated feedback control of the sawtooth period by actuating on the EC launcher injection angle in order to obtain the sawtooth period at a pre-determined value [140, 141] or to maximise the sawtooth period [143]. Figure 10 shows the sawtooth period as a function of time when real-time control using ECCD is applied in TCV. It is evident that by changing the launcher angle, and therefore modifying the magnetic shear around $q = 1$, the observed sawtooth period can be forced to track a requested period. The time lag between the change in the requested period and that achieved is determined by the nonlinear plasma response and movement of the $q = 1$ radius. It should be noted that the real-time controller algorithm in these TCV experiments is based upon a prior knowledge of sawtooth destabilisation with respect to launcher angles which educates the control system. Conversely, Tore Supra have implemented a ‘search and maintain’ control algorithm to vary the ECCD absorption location in search of a location

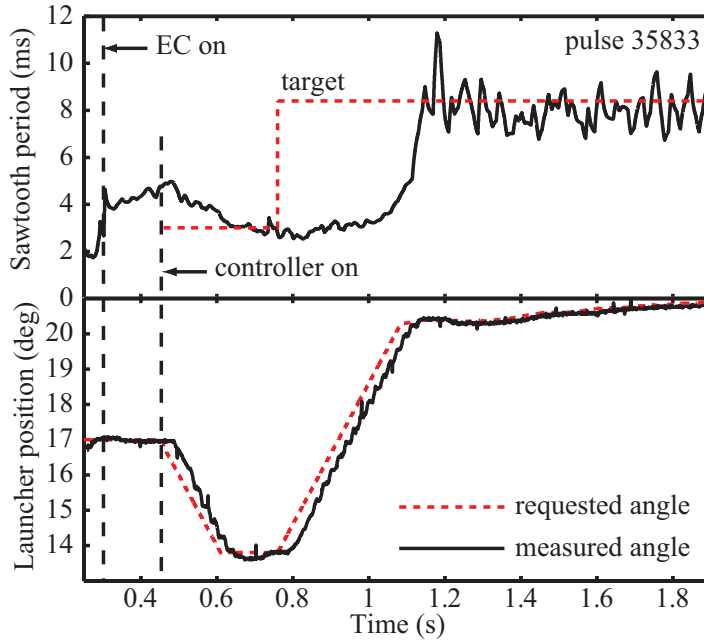


Figure 10. The sawtooth period observed in TCV when real-time ECCD control is applied. The control algorithm successfully achieves and tracks two levels of requested sawtooth period by moving the ECH launcher angle to change the deposition location, and consequently the magnetic shear at $q = 1$ accordingly. *Paley et al* “Realtime control of the sawtooth period using EC launchers” *Plasma Phys. Control. Fusion* **51** 055010 (2009) [141] published by Institute of Physics Publishing.

at which the sawteeth are minimised; having achieved this, the controller maintains the distance between the ECCD deposition location and the measured inversion radius despite perturbations to the plasma [142].

The remaining concern about current drive control is whether changes in s_1 can overcome the stabilisation arising in the presence of energetic particles. In ITER, the fusion-born α particles are likely to give rise to a large δW term, as described in section 2.1. This means that the change in the magnetic shear may need to be substantial to compete with the kinetic stabilisation, especially if the fast ions arising from concurrent ICRH and NBI heating exacerbate the situation. As such, recent experiments have attempted to destabilise sawteeth using ECCD in the presence of energetic particles. Sawtooth destabilisation of long period sawteeth induced by ICRH generated core fast ions with energies $\geq 0.5\text{MeV}$ has been achieved in Tore Supra, even with modest levels of ECCD power [133]. Figure 11 shows the sawtooth period in two Tore Supra discharges, one with just ICRH heating in the plasma core, and a second with additional ECCD swept across the $q = 1$ radius. The ICRH fast ions lead to long sawtooth periods, but despite the presence of these highly energetic ions, the ECCD is able to drop the sawtooth period back to a level approaching that observed in Ohmically heated plasmas when the deposition is optimally located just inside the $q = 1$ surface. Similarly, ECCD destabilisation has also been achieved in the presence of ICRH accelerated NBI ions in ASDEX Upgrade [144] as well as with normal NBI fast ions in ASDEX Upgrade [119],

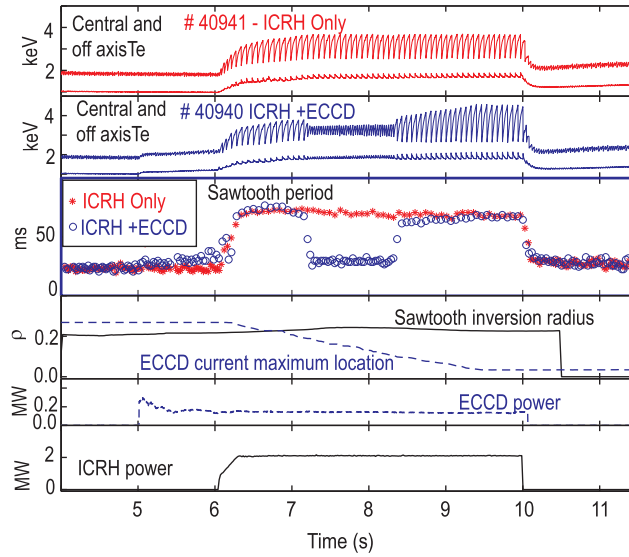


Figure 11. Demonstration of sawtooth destabilization in the presence of core fast ions in Tore Supra. Two consecutive shots with 2.3 MW of ICRH with and without co-ECCD are shown. The radial ECCD deposition location was scanned from outside the sawtooth inversion radius to the plasma center. When the deposition was just inside $q = 1$ the sawtooth period dropped to approximately the level of Ohmically heated plasmas, despite the stabilising ICRH ions in the plasma core. Reprinted figure with permission from Lennholm *et al* Phys Rev. Lett., **102** 115004 (2009) [133]. Copyright 2009 by the American Physical Society.

JT-60U [129] and HL-2A [145]. Despite these promising results, destabilisation of monster sawteeth in the presence of a significant population of highly energetic particles at high β_h has yet to be demonstrated and remains a key goal of ongoing sawtooth control activity.

Finally, it should be noted that other current drive actuators can also affect sawtooth behaviour. For instance, Lower Hybrid Current Drive has been used to control sawteeth [146–148], as has Mode Conversion Current Drive (MCCD) [149, 150]. Figure 12 shows the sawtooth period as a function of the radial location of the mode conversion layer in Alcator C-Mod plasmas as the toroidal field is varied to move the resonance from inside to outside the inversion radius. In accordance with the ECCD experiments, the change in the local magnetic shear due to MCCD causes the sawtooth period to increase then decrease as counter-currents are driven first inside then outside $q = 1$. Conversely, the co-current phasing and symmetric phasings result in a decrease and subsequent increase in sawtooth period, symptomatic of a reversal of the driven current and thus opposite change in s_1 . Simulations with the full wave code TORIC indicate that the electron heating and current drive are due to mode converted ion cyclotron

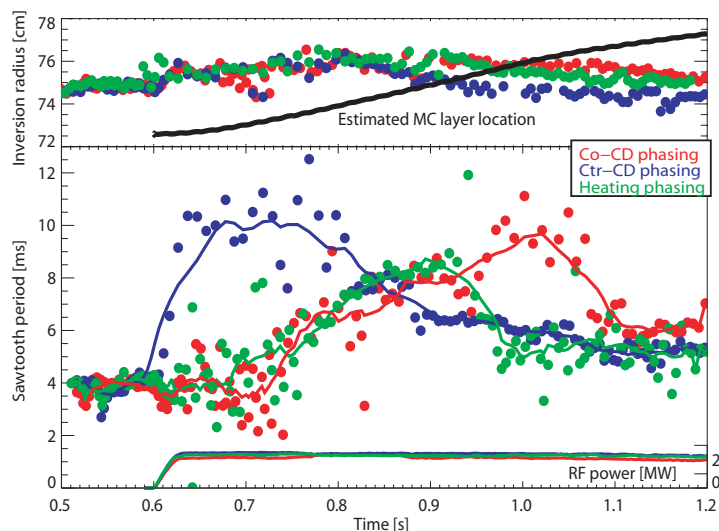


Figure 12. Sawtooth control via changing the magnetic shear by mode conversion current drive demonstrated on Alcator C-Mod. As the mode conversion layer is moved from inside to outside the inversion radius, the sawtooth period is found to increase then decrease for counter-current drive phasing. For both co-propagating ICRH waves and pure heating phasings the sawtooth period decreases then increases. The symmetric phasing results in a co-current due to the strong up-down asymmetry. Reprinted figure with permission from Parisot *et al* “Sawtooth period changes with mode conversion current drive on Alcator C-Mod” *Plasma Phys. Control. Fusion* **49** 219 (2007) [150] published by Institute of Physics Publishing.

waves, and that the driven currents dominantly determine the sawtooth behaviour [150]. Modulated ECH has also been considered theoretically as a tool to dynamically stabilise the $m = 1$ tearing mode for sawtooth control [151] and has had some experimental support [152, 153] Non-inductive currents driven by NBI and ICRH are discussed in the context of sawtooth control in sections 4 and 5 respectively.

4. Neutral Beam Injection

Neutral beam injection affects sawtooth behaviour through both the introduction of energetic particles as well as the torque applied to the plasma. Having said that, NBI is not considered as a sawtooth control actuator for ITER for two reasons: Firstly, the broad $q = 1$ radius expected in the ITER baseline operating scenario means that the fast ions resulting from NBI will always be inside $q = 1$, and thus, although strongly stabilising, unable to *destabilise* the sawteeth. Secondly, the predicted rotation in ITER is small [55], meaning that the gyroscopic stabilisation of the kink mode is likely to be a negligible effect.

Nonetheless, recent experiments concerning sawtooth stability in NBI-heated plasmas have significantly enhanced our understanding of the physical mechanisms that dictate mode stability, as well as providing a tool for sawtooth control in present-day devices. It has been known for some time that NBI heating could strongly stabilise the

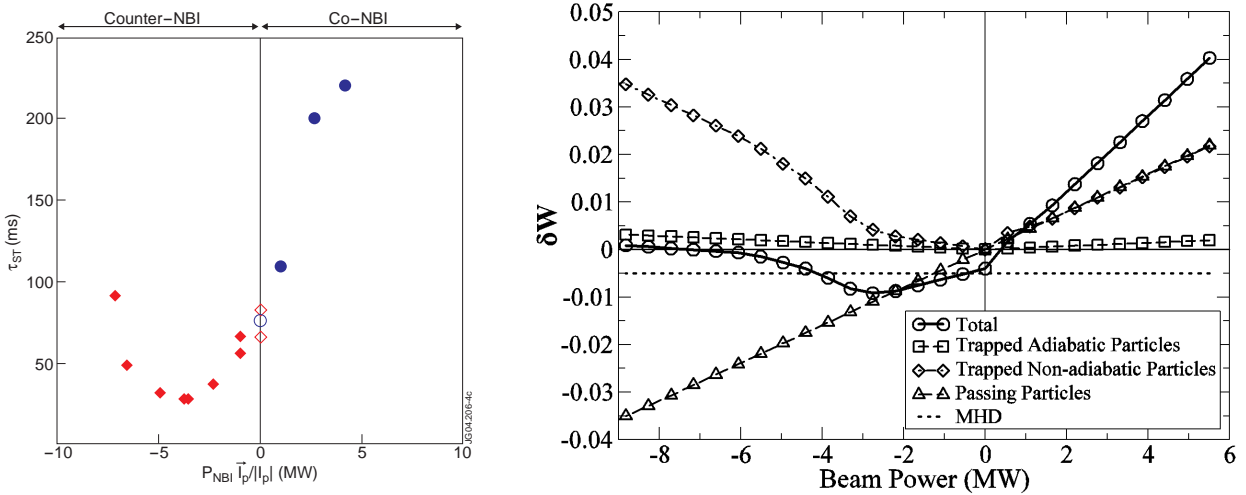


Figure 13. (left) Sawtooth period in JET NBI-heated plasmas as a function of P_{NBI} . Here, negative power means injected counter- I_p . Reproduced with permission from Nave *et al* Physics of Plasmas **13** 014503 (2006) [155] Copyright 2006, American Institute of Physics, and (right) The contribution to δW from each energetic particle species with respect to injected beam power for a JET equilibrium (discharge 60998) including flow shear effects. It is evident that the minimum in δW occurs in the counter-NBI regime for similar P_{NBI} as the minimum in sawtooth period. Reproduced with permission from Chapman *et al* Physics of Plasmas **14** 070703 (2007) [156] Copyright 2007, American Institute of Physics.

kink mode and lead to long sawtooth periods [10], an effect attributed to the stabilisation arising in the presence of a population of core energetic trapped ions, as described in section 2.1.1, as well as stabilisation occurring in strongly rotating plasmas, as outlined in section 2.2. However, JT-60U reported that application of 350keV Negative-ion neutral beam injectors (N-NBI) led to strong stabilisation of sawteeth [154], despite the fact that at such high beam energy, the resulting fast ion population is predominantly passing. This led theorists to suggest that circulating ions could also influence the stability of the $n = 1$ internal kink mode. As described in section 2.1.2, destabilisation of the internal kink mode can occur when $\partial f_h(v_{\parallel} > 0)/\partial r > \partial f_h(v_{\parallel} < 0)/\partial r$, which occurs when the energetic ions are injected either off-axis ($\partial f_h/\partial r > 0$) and oriented with the plasma current, or when the fast ion population is predominantly on-axis ($\partial f_h/\partial r > 0$) and directed opposite to the plasma current. This effect has been demonstrated by experiments that exhibit an asymmetry in sawtooth behaviour depending upon whether the NBI is injected co- I_p , or counter-current. The sawtooth period in JET was observed to lengthen as the injected co-NBI power was increased, but to decrease to some minimum before subsequently lengthening as more NBI power was injected counter- I_p [155], as illustrated in figure 13. This asymmetric behaviour is in excellent accordance with the theoretical prediction that when the NBI fast ion population is peaked in the plasma core, the co-transiting ions are stabilising whereas the counter-passing ions are destabilising, resulting in a shorter sawtooth period. Detailed drift kinetic modelling of the effect of the JET NBI ions on the stability of the internal kink mode has shown that

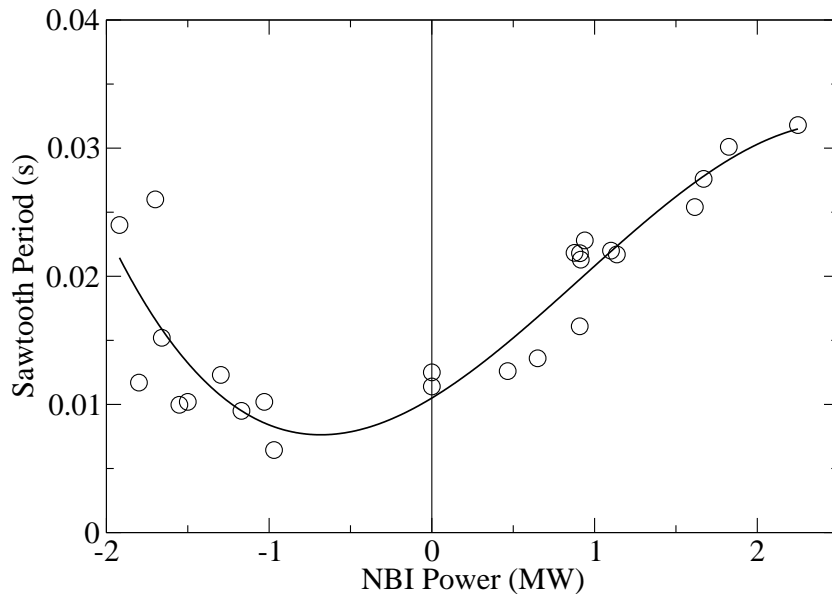


Figure 14. Sawtooth period for MAST discharges as a function of applied NBI power. $I_P \in [680, 740]$ kA, $B_T \in [0.35, 0.45]$ T and $n_e \in [1.6, 2.3] \times 10^{20} \text{m}^{-3}$. Negative beam power is taken to represent NBI power in the counter- I_P direction. Reproduced with permission from *Chapman et al* [68].

the contribution from the passing fast ions (which account for the majority of the NBI population) is of the same order of magnitude as the stabilising effect of the trapped fast ions [156]. Figure 13 also illustrates that the asymmetry observed experimentally is explained by the competition between the stabilising trapped ions and the destabilising counter-passing ions in the counter-NBI regime, compared with two complementary stabilising effects for co-NBI, and that the minimum in sawtooth period is replicated by the minimum in $\delta\hat{W}$ calculated by sophisticated numerical modelling. The minimum in the sawtooth period is only explicable with the inclusion of flow shear effects. Whilst the amplitude of the rotation is strongly sub-Alfvénic, such that gyroscopic effects as outlined in section 2.2 play a small role, the flow *shear* at $q = 1$ can be significant, and reduces the stabilising effect of the trapped ions when $\Delta\Omega < 0$, as explained in section 2.1.1. Whilst it was initially surprising that finite orbit width of these relatively low energy NBI passing ions could play such an important role in determining sawtooth stability, this was later explained by the fact that the orbit width of the passing ions increases as the pitch angle approaches the trapped-passing boundary [60–62]. Consequently the significant fraction of barely passing ions arising from neutral beam injection in JET have a large effective orbit width, and thus strongly influence sawtooth behaviour.

Experiments in MAST [68] and TEXTOR [157] also exhibited an asymmetry in the sawtooth period with respect to the injected NBI power when oriented either co- or counter-current. Figure 14 shows this observed asymmetry in sawtooth period in NBI-heated plasmas in MAST. However, in these smaller devices, the effect of rotation can

become increasingly significant. Whilst the fast ions do have a stabilising influence, the significant trapped fraction in spherical tokamaks is stabilising in either co- or counter-NBI regimes, meaning that kinetic effects cannot explain the experimentally observed minimum in sawtooth period. On the other hand, the smaller moment of inertia and high beam power per unit volume in spherical tokamaks result in rotation speeds which approach the ion sound speed [63]. Such strong toroidal rotation results in sawtooth stabilisation, with the minimum in sawtooth period in the counter-NBI regime explained by relative direction of the flow induced by the NBI with respect to the intrinsic rotation of the plasma dominated by the ion diamagnetic drift [68, 158]. In TEXTOR, the sawtooth period reaches a minimum with a low level of co-NBI and a maximum in the counter-NBI regime [157]. This is due to a competition between the gyroscopic stabilisation of the kink mode and the destabilisation arising in the presence of counter-passing fast ions.

Numerical modelling to assess the stabilising contributions from both NBI-induced torques and from the resultant passing fast ion population has improved significantly in recent years. Angioni *et al* [103] considered the role played by on-axis co-NBI fast ions in lengthening the sawtooth period in JET. By assessing each of the triggering criteria given in equations 7 to 9 using the PRETOR transport code, the nonlinear evolution of the sawtooth cycle could be predicted, and the observed sawtooth period was compared favourably with the numerical predictions given by the linear crash trigger model outlined in section 2.5. More recently, the assessment of the kinetic contribution to the internal kink mode stability has been improved through the use of drift kinetic codes including finite orbit width effects. For instance, the role of both the trapped fast ions and the passing fast ions has been compared using the Monte-Carlo guiding centre HAGIS code [159] in JET [24, 156]. Such accurate calculation of the kinetic effects has facilitated an assessment of the stabilisation arising from the α particles and beam fast ions in ITER [23, 24], both of which are likely to incur very long sawtooth periods. Finally, the effect of toroidal rotation on the stability of the internal kink mode has also been assessed numerically [70, 158] and found to be important in determining sawtooth behaviour in fast rotating spherical tokamak plasmas [68].

Following the experimental and numerical verification of the importance of passing fast ions in determining sawtooth stability and the observation that different NBI tangency radii led to different sawtooth behaviour [119], experiments were conducted to test whether off-axis co-NBI could be used to deliberately destabilise the internal kink mode. Experiments in JET showed that the application of off-axis NBI such that the peak of the fast ion population was deposited outside the $q = 1$ surface led to a destabilisation of the sawteeth [160]. Furthermore, sawtooth control using off-axis NBI was also demonstrated in the presence of a concurrent stabilising fast ion population in the plasma core [161]. Figure 15 shows that when ancillary off-axis NBI power is applied in JET discharge 58855, the sawtooth period decreases by a factor of three compared to the on-axis NBI only phase, despite an overall increase in β_h leading to stronger stabilisation from the trapped ions. Numerical modelling, which is also shown in

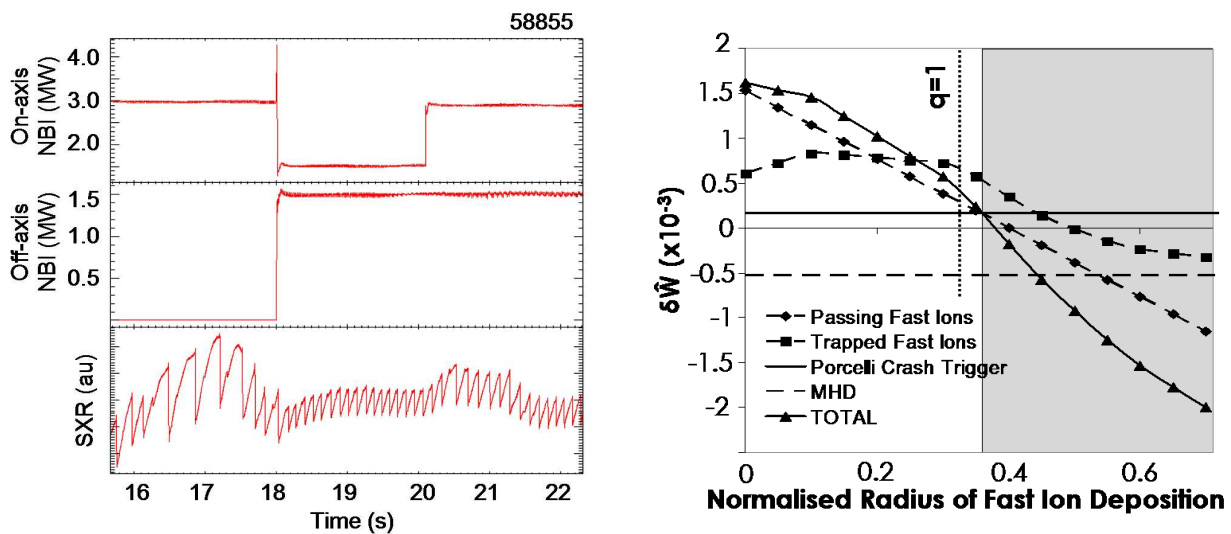


Figure 15. (left) The soft X-ray emission and beam heating waveforms for JET shot 58855. The sawtooth period is significantly shorter when the total β_h is kept constant, but some off-axis NBI is used in place of on-axis heating. Further, this discharge also shows that the application of ancillary off-axis NBI can decrease the sawtooth period, despite an overall increase in β_h . *Chapman et al* [161]. (right) The potential energy of the internal kink mode as a function of the deposition location of the centre of the fast ion population. When the fast ions are centred just outside the $q = 1$ surface, they destabilise the kink mode and consequently trigger sawteeth more frequently. Equations 7-10 suggest that a sawtooth crash will occur within the shaded region. *Chapman et al* “Sawtooth control using off-axis NBI” *Plasma Phys. Control. Fusion* **50** 045006 (2008) [160] published by Institute of Physics Publishing.

figure 15, confirmed that the passing fast ion effects dominantly determine the sawtooth behaviour, and the change in the magnetic shear arising from the broad neutral beam current drive is negligible in comparison.

In addition to the demonstration of the effect of off-axis NBI on sawtooth behaviour in JET, confirmation of the dominance of passing fast ion effects was also achieved in MAST and ASDEX Upgrade experiments which altered the radial gradient of the fast ion pressure at the $q = 1$ surface, and so changed the destabilising effect. The destabilisation from the passing ions has been shown to be sensitive to the location of $q = 1$ with respect to the peak of the deposition of the fast particles. In MAST this was achieved by displacing the plasma vertically such that the beam deposition begins inside $q = 1$ but moves to well outside the $q = 1$ surface [162]. In ASDEX Upgrade, the trajectory of the most off-axis positive ion neutral injector (PINI) has been changed in order to move the deposition location of the energetic ions whilst keeping the plasma conditions relatively unchanged. Figure 16 shows the beam trajectories for different inclinations of the off-axis PINI and the corresponding sawtooth behaviour measured by soft X-ray emission. The passing energetic ions led to maximum destabilisation when the $q = 1$ surface is well inside the beam deposition location. This means that it is unlikely that off-axis NBI could be realistically utilised as a sawtooth control mechanism since

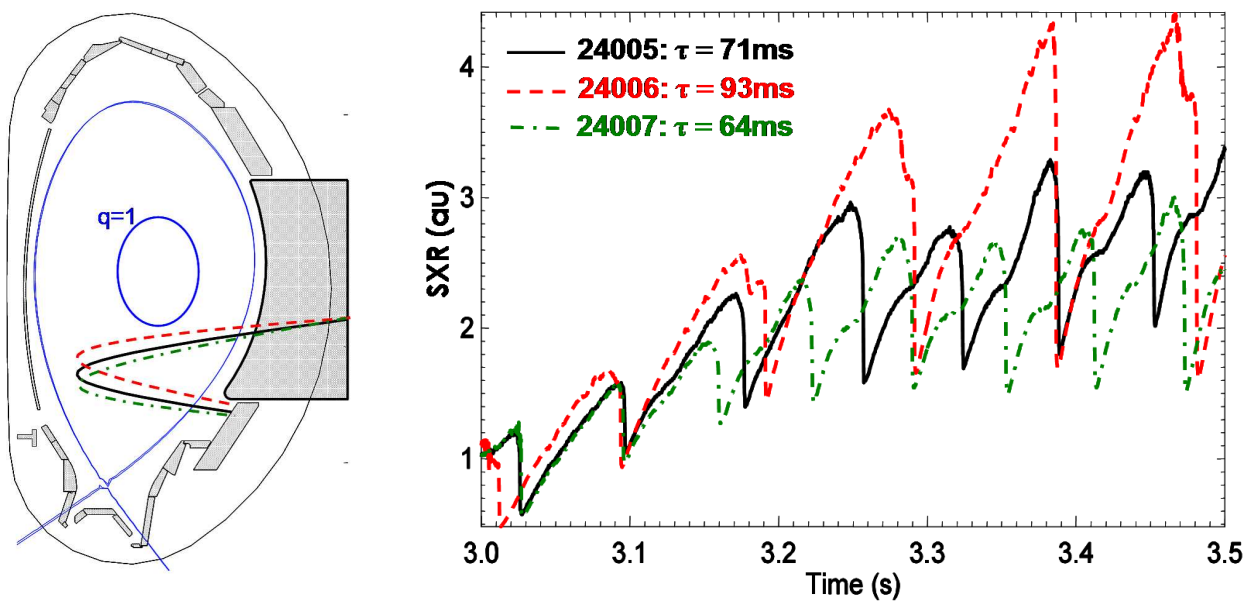


Figure 16. (left) The beam trajectories of the off-axis PINI in ASDEX Upgrade as the PINI is tilted on its support. Also shown for comparison is the approximate position of the $q = 1$ surface, and (right) the corresponding soft X-ray emission in three ASDEX Upgrade plasmas. The sawtooth period decreases as the beam is injected further off-axis. Discharge 24006 represents the most on-axis NBI heating and shot 24007 is the most off-axis. Reproduced with permission from Chapman *et al* Physics of Plasmas **16** 072506 (2009) [162] Copyright 2009, American Institute of Physics.

$q = 1$ must be very core localised and even then, the destabilisation from kinetic effects must overcome gyroscopic stabilisation resultant from NBI torque.

5. Ion Cyclotron Resonance Heating

It has been known for some time that the application of ion cyclotron resonance heating has a significant effect on the sawtooth behaviour. High power ion cyclotron resonance heating (ICRH) experiments were conducted in JET, in which the sawtooth instability was suppressed for seconds [33] and long sawtooth quiescent periods were terminated abruptly by a sawtooth collapse that followed the switch off of the ICRH [34]. Following these observations, early experiments focussed on suppressing or delaying the first sawtooth crash through the presence of core fast ions born due to ICRH. On-axis ICRH was found to result in monster sawteeth, which often triggered NTMs [10, 163]. The long sawtooth periods and giant crashes were shown to be consistent with strong kinetic stabilisation through peaked fast ion pressures [38–40, 164] despite an increase in the destabilising toroidal effects resulting from an increase in the pressure [165, 166]. This enhanced confidence in the applicability of kinetic-fluid theory [36, 42] for modelling sawtooth behaviour in RF heated plasmas. Soon after, experiments with ICRH heating located off-axis showed that sawtooth destabilisation could also be achieved [114, 115]. Following these demonstrations of sawtooth destabilisation, control of sawteeth by ICCD

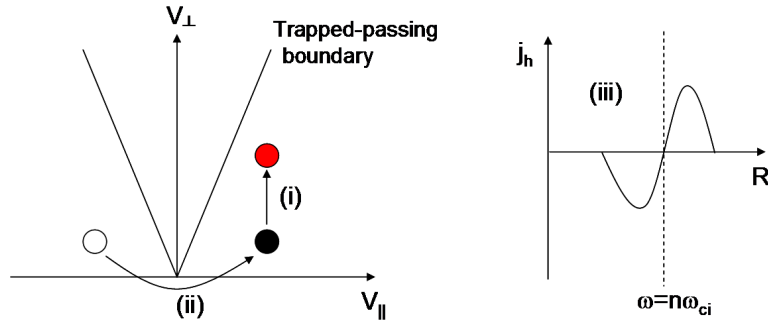


Figure 17. A schematic illustration of ICCD arising from a forward propagating wave ($k_{\parallel} > 0$) interacting with ions of the low-field side of the cyclotron resonance. (i) Particles with $v_{\parallel} > 0$ are accelerated in the perpendicular direction. Collisional pitch angle scattering acts to restore the isotropic distribution, but since scattering scales with v^{-3} , (ii) there is an effective transfer of ions from the $v_{\parallel} < 0$ region to the $v_{\parallel} > 0$ region, which (iii) results in a driven current with a dipole structure.

has been widely exploited on JET [12, 26, 167–170]. Two ICCD schemes have been used, namely (i) minority ICCD where a minority ion species resonates with the fundamental cyclotron frequency of the ICRH wave, absorbing the RF power and carrying the fast ion current, and (ii) second harmonic ICCD, where an ion species (not necessarily a minority species) resonates at its second harmonic cyclotron frequency, $\omega = 2\omega_{ci}$ with the RF waves. Recent results from Alcator C-Mod have also shown the effectiveness of mode conversion current drive for affecting the sawtooth behaviour by efficient electron heating close to the $q = 1$ surface and consequently local current profile modification [149, 150].

Whilst the strong stabilisation arising from on-axis ICRH energetic ions was attributed to the trapped fast ion effects [45] and increase in fast ion pressure peaking [38], the destabilisation arising from off-axis ICRH was attributed to the non-inductively driven currents. The current drive resulting from resonant minority wave-particle interactions at cyclotron frequencies, or majority ions at harmonics of the cyclotron frequency, relies on an asymmetry in the passing ion distribution induced by directed wave spectra (ie waves propagating preferentially in one direction) and on the velocity dependence of the collisional pitch angle scattering [116]. The resonance condition between a wave and the cyclotron motion of the resonant particles is given by $\omega - n\omega_{ci} - k_{\parallel}v_{\parallel} = 0$, meaning that preferentially propagating waves can resonate with either co-transiting or counter-transiting ions, depending on the direction of wave propagation and the location of the interaction with respect to the cyclotron resonance. For example, consider a forward-propagating wave ($k_{\parallel} > 0$) interacting with passing ions on the low-field side of the resonance. The wave can only interact with particles with $v_{\parallel} > 0$ and accelerates them mainly in the perpendicular direction. Consequently there is a depletion of co-passing ions in the bulk distribution, and an enhanced co-passing high energy population. Whilst collisional pitch angle scattering will restore the isotropic distribution, the strength of the scattering scales as v^{-3} , and so there is an effective transfer of ions from the $v_{\parallel} < 0$ region to the $v_{\parallel} > 0$ region, resulting

in a driven current. This process is illustrated schematically in figure 17. The Fisch model [116] predicts that waves propagating in the co-current direction ($k_{\parallel} > 0$) result in ICCD with a dipole structure with a positive part with respect to the plasma current on the low-field side of the cyclotron resonance and a negative lobe on the high field side. For counter-propagating waves, the currents in the dipole structure change sign. This mechanism is reviewed succinctly in references [114] and [169]. This classical model does not include finite orbit width effects of the resonating ions, acceleration of ions by waves in the parallel velocity, or trapped ions, and when such effects are included, ancillary current drive mechanisms are found [60, 117, 118, 164, 169, 171]. Since the Fisch model for ICCD relies on passing ions to carry the current, it is important that not too many resonating ions are driven into trapped orbits. This is achieved by having an effective ‘tail temperature’ (average of non-thermal ions) of the resonating ions at the energy where collisions with ions and electrons are equally likely. However, in JET plasmas the tail temperature is typically much larger, so non-classical effects concerning finite orbit widths and wave induced spatial diffusion tend to dominate the driven current profiles, such that numerical calculations capable of including such effects are necessary for accurate determination of the ICCD.

As with the early ECCD sawtooth control experiments outlined in section 3, the first ICRH destabilisation experiments employed field and current ramps to sweep the ICRH resonance location across the inversion radius, and consequently change the magnetic shear in and around the $q = 1$ surface. However, the change in the magnetic shear at $q = 1$ resulting from the ICCD dipole perturbation is complicated by the fact that the $q = 1$ surface is moved radially when the current perturbation is swept across. Consider the case of the resonance location of a counter-propagating wave on the high-field side (ie with a negative current lobe of the dipole nearest the axis) being swept from outside to inside the $q = 1$ surface. As the negative current lobe gets to the initial location of $q = 1$, this surface is displaced towards the axis, whilst the negative current increases q just outside the rational surface and so increases s_1 . The reduction in r_1 means that the fast ion pressure within $q = 1$ has decreased, which together with the strong increase in magnetic shear at $q = 1$ means that counter-propagating waves on the high-field side just outside $q = 1$ are expected to be destabilising. Repeating the argument for a co-propagating wave just outside $q = 1$, the decrease in magnetic shear and increase in r_1 implies stabilisation. A cartoon illustrating this is given in figure 9 of reference [169], and is indeed what is observed in JET plasmas. Figure 18 shows the sawtooth behaviour in two JET pulses as the resonance of co-propagating ICRH waves ($+90^\circ$ phasing of the ICRH antenna) and counter-propagating waves (-90°) is swept across the $q = 1$ radius. The $+90^\circ$ ICCD results in a strong stabilisation as the resonance is just outside the inversion radius since the shear is reduced, and even more stabilisation as the ICRH moves inside $q = 1$ due to the increase in fast ion pressure. Conversely, the -90° ICCD results in marked destabilisation with the resonance just outside $q = 1$ before an increase in sawtooth period is observed when the ICRH is well inside $q = 1$ and the trapped fast ion stabilisation begins to dominate. It should be noted that ICRH wave induced pinch

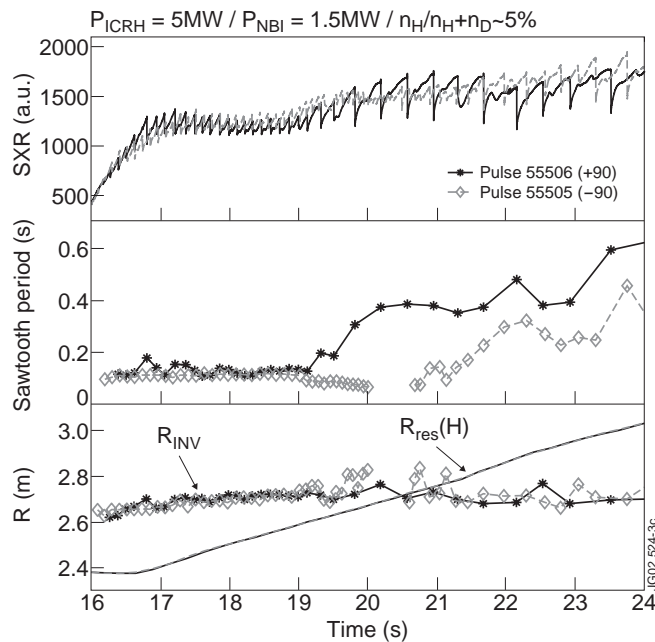


Figure 18. The sawtooth behaviour during JET pulses with co-propagating ICRH waves (+90°) and counter-propagating waves (-90°) as the resonance layer is moved across the inversion radius. The sawteeth are destabilised by the -90° ICCD just outside $q = 1$ before the increase in fast ions results in stabilisation when the resonance is well inside $q = 1$. The +90° waves are strongly stabilising when the resonance is both just outside and inside $q = 1$. Reproduced with permission from Mayoral *et al* Physics of Plasmas **11** 2607 (2004) [26] Copyright 2004, American Institute of Physics.

in the presence of an asymmetric distribution results in a more peaked fast ion pressure for co-moving waves [164], leading to stronger stabilisation from on-axis heating, as observed.

It has since been shown on JET that ICRH is effective in keeping the sawtooth period short even in the presence of a substantial core fast-ion population [168]. Figure 19 shows the sawtooth behaviour in JET discharge 58934 where +90° ICRH is applied in the plasma core, resulting in fast-ion stabilised sawteeth, which are successfully destabilised by concurrent -90° ICCD near the $q = 1$ surface [168, 169]. Furthermore, ICCD control has also been demonstrated in plasmas with even more heating power on-axis from neutral beam injection and much higher β_p , well above the critical threshold for triggering of 3/2 NTMs in the absence of sawtooth control [172].

Due to the complex dipole nature of the ICRH driven current, detailed modelling has been conducted to assess the relative roles of the change in the magnetic shear and the energetic ions. For instance, the PION [173] and FIDO [174] ICRH codes were used to produce the resonating fast ion distribution and the ICCD profile, which was then input into the PRETOR transport code including the sawtooth trigger model to assess sawtooth stability. This detailed wave modelling showed that an ICRH resonance on the high field side led to optimised conditions for the classical Fisch model as the fast ion orbits are closer to the passing-trapped boundary. Conversely, a low field side ICRH resonance

results in the ICCD being dominated by finite orbit width effects of trapped ions [117] which gives rise to a decrease in the magnetic shear near the resonance, independent of antenna phasing. This independence of direction of propagation of low field side ICRH is manifest experimentally, and the observed sawtooth period has been replicated well by PRETOR modelling during a sweep of the resonance position [170]. Numerical modelling suggested that in the JET ICCD experiments, the destabilisation of the sawteeth occurred primarily due to a change in the magnetic shear at $q = 1$ [114, 167, 169, 170], as with the current drive schemes outlined in section 3.

However, it has since been noticed that the sensitivity of sawtooth destabilisation required accuracy of the resonance position with respect to the $q = 1$ surface of less than 0.5% (ie within 1cm of the $q = 1$ surface in JET) [172], which is far more sensitive than expected from the control mechanism involving a modification of the magnetic shear. In order to explain this, the kinetic effects of the passing ions outlined in sections 2.1.2 and 4 have recently been extended across all of velocity space, including barely passing trajectories. Graves *et al* showed that the sawtooth control mechanism responsible for localised off-axis toroidally propagating waves is due to the radial drift excursion of the energetic ions distributed asymmetrically in the velocity parallel to the magnetic field [60]. Furthermore, the ICRH induced energetic particles are more effective at controlling the sawteeth than the passing fast ion effects arising from neutral beam injection described in section 4 because the orbit widths of the energetic ions are larger and the parallel asymmetry of the fast ion distribution is more strongly radially sheared. Early modelling using a bi-Maxwellian distribution to represent the ICRH fast ions [175] indicated the strong effects of the pressure anisotropy of the passing ions [24, 176]. Subsequently, the effect of asymmetry in the distribution has also been considered through detailed SELFO [177] RF wave-field and fast ion distribution function simulations coupled with the drift kinetic HAGIS code, which confirmed the effective nature of the kinetic mechanism for sawtooth control [62]. Indeed, the counter-propagating waves deposited on the high field side just outside the $q = 1$ surface in JET shot 58934 (illustrated in figure 19) give rise to a fast ion destabilising effect which drives the internal kink mode ideally unstable. In contrast, the change in the magnetic shear has only a moderate effect on resistive stability. Finally, the kinetic mechanism also results in a deep and narrow minimum in the change of the potential energy when the peak of the passing fast ion distribution is just outside the $q = 1$ surface. This narrow destabilising effect explains the extreme sensitivity of the sawtooth behaviour to the deposition location of the ICRH waves.

Following the proposal of this kinetic mechanism to describe the highly effective and strongly localised nature of sawtooth control arising from toroidally propagating ICRH waves with off-axis resonance, dedicated experiments in JET aimed to differentiate between the fast ion and conventional current profile modification effects [60, 61]. The change in the equilibrium current due to the ICRH is negligible when ^3He minority heating scheme is employed in a deuterium majority plasmas where the current dragged by the background plasma tends to cancel the ^3He current [114, 116, 178]. Recent

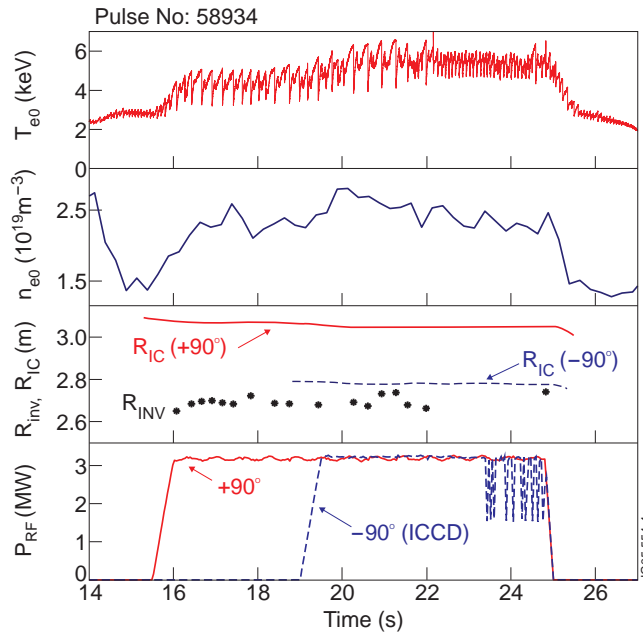


Figure 19. The sawtooth behaviour during JET discharge 58934. When $+90^\circ$ ICRH is applied in the plasma centre the sawtooth period is significantly lengthened. Concurrent -90° ICCD near the $q = 1$ surface results in a destabilisation of the fast ion stabilised sawteeth. Reprinted figure with permission from Eriksson *et al* Phys. Rev. Lett., **92** 235004 (2004) [168]. Copyright 2004 by the American Physical Society.

JET experiments using such ^3He minority heating on the high-field side just outside the $q = 1$ surface lead to a strong destabilisation for counter-propagating waves (-90°) and a strong stabilisation for co-propagating waves ($+90^\circ$), as illustrated in figure 20. In both discharges, an on-axis population of NBI fast ions induce relatively long period sawteeth. For the -90° phasing the sawtooth period is reduced to nearly the level of Ohmic sawteeth, whereas $+90^\circ$ increases the sawtooth period significantly, with the longest period of over 1s triggering an $n=2$ NTM. Numerical modelling has provided detailed verification that the fast ion mechanism is consistent with the sawtooth behaviour in these plasmas [61]. Furthermore, more advanced confirmation was attained experimentally by varying the amplitude of the fast ion mechanism by changing the concentration of the minority ions. Figure 21 shows the sawtooth behaviour in three different JET discharges, two with low concentration and a third with high concentration with -90° phasing ICRH. It is clear that, whilst the radial space over which the fast ions can destabilise the mode is approximately the same, the application of ICRH does not affect the sawtooth period as strongly for high minority concentration ($n_h/n_e = 0.03$). This strong sensitivity to minority concentration is also seen in stability calculations, as seen in figure 21. For $n_h/n_e = 0.01$, the destabilising effect of the ICRH energetic passing ions dominates over the stabilising effect of the core NBI ions, as manifest by a reduction in sawtooth period in discharge 78737. Conversely, at very low concentration ($n_h/n_e = 0.0015$) the minority power absorption is reduced and higher minority ion energies give rise to a broader fast ion distribution and enhanced losses, reducing the

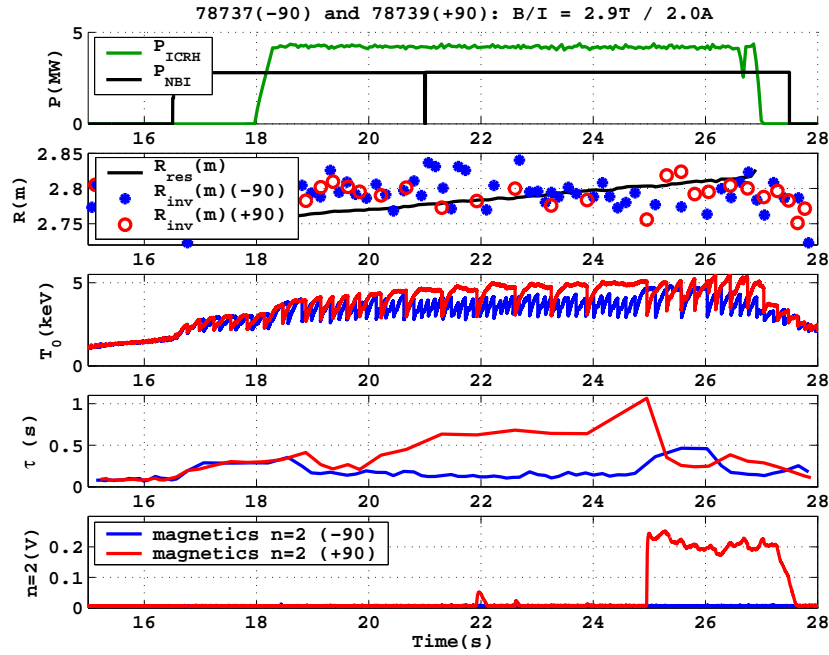


Figure 20. JET pulses 78737 and 78739 with -90° and $+90^\circ$ ICRH off-axis respectively. The NBI fast ions in the core lead to long sawtooth periods. When the He^3 minority heating is deposited off-axis, the fast ions destabilise the sawteeth with -90° phasing, but stabilise them with $+90^\circ$ phasing, to the extent that a 1s long sawtooth triggers an NTM. Reproduced with permission from *Graves et al* [61].

impact on sawtooth stability. Similarly, when the minority density is too high the effect of the ICRH ions is much smaller than the combined effect of NBI fast ions and fluid drive due to the reduced effective orbit width at higher concentration. This is seen in discharge 78740 where the application of counter-propagating ICRH waves does not strongly alter the sawtooth behaviour [61].

The fact that off-axis passing fast ions with large orbit widths due to toroidally propagating ICRH waves can directly, and dramatically alter the sawtooth period is encouraging for ITER baseline scenario operation. Previous studies of the ion cyclotron current drive in ^3He minority schemes, which are primarily expected in ITER [8,178], predict that drag currents will result in negligible driven current [114,178]. Consequently, ICRH was not envisaged for ITER since control via perturbations to the magnetic shear at the $q = 1$ surface are expected to be small. However, the recent development in the understanding of the effects of large orbit width passing fast ions near the passing-trapped boundary supported by experimental evidence using ^3He minority ICRH in JET, suggests that ICRH can be a useful tool for sawtooth control in ITER. The benefit of this mechanism is that it directly reduces the change in potential energy of the internal kink mode, meaning that a small change in the magnetic shear due to concurrent current drive schemes is more likely to successfully destabilise the sawteeth, as seen in equation 9. However, since the resonance position of the ICRH must be so precisely localised with respect to the rational surface, real-time feedback is highly

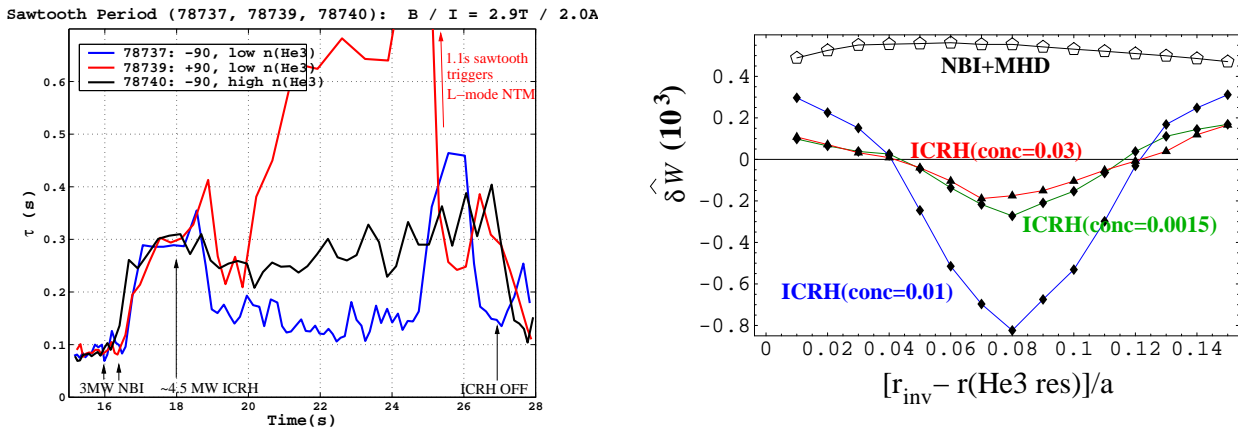


Figure 21. (left) JET experiments showing that the fast ions due to He³ ICRH heating just outside $q = 1$ (de)stabilise the sawteeth for (-)+90° phasing respectively for low He³ concentration, but barely affect the sawtooth period at high concentration. This is replicated by drift kinetic modelling (right) which shows that the change in potential energy of the kink mode for trace concentration and for 3% is negligible, whereas for 1% concentration there is a strong and radially local effect. Reproduced with permission from *Graves et al* [61].

desirable for practical sawtooth control. Initial real-time studies have begun in JET by varying the ICRH frequency [179].

6. Discussion and Implications for ITER

Developments in the understanding of sawtooth control techniques have shown that current drive schemes, neutral beam injection and RF heating can all stabilise or destabilise sawteeth, with different effects depending on whether core or off-axis heating is applied. Whilst there has been considerable advancement in both the theoretical understanding and numerical prediction of sawtooth physics and the experimental techniques for sawtooth control, there remain a number of open questions for sawtooth control in burning plasmas. Among these are (i) what will the sawtooth period be in ITER?; and (ii) what is the maximum sawtooth period permitted without triggering an NTM? An early answer to the first question was proposed in reference [22] where the linear stability thresholds outlined in section 2.5 were simulated using a 1-d transport solver, indicating a full reconnection sawtooth period of 100s with a $q = 1$ radius of 50% of the plasma minor radius. Indeed, a similar answer is arrived at by extrapolating monster sawteeth observed on JET [10] by the resistive diffusion time to ITER [75]. Since then, the same crash trigger model has been implemented in more accurate transport codes. Modelling using TSC [180] with H-mode profiles given by either the multi-mode model [181] or the Gyro-Landau fluid model GLF23 [182] predicted 50s sawtooth period for the complete reconnection model and 2-3 times shorter periods for partial reconnection, with a $q = 1$ radius of 42% of the minor radius (which agrees well with the inversion radius predicted in BALDUR modelling [183]). Finally,

time-dependent integrated predictive modelling with the PTRANSP code predicted a sawtooth period much less than 50s [184]. All of these predictions entail sawteeth with a quiescent period much longer than the energy confinement time. Whilst the sawteeth have a negligible effect on the stored energy or the rate of neutron production, it is the possibility that sawteeth with $\tau_s \gg \tau_E$ could trigger NTMs which is of primary concern. The second issue of whether a sawtooth period in the range of 20-50s will avoid triggering NTMs is currently poorly understood, though empirical scaling of sawtooth-triggered NTMs in current devices may provide a rudimentary answer [185].

Nonetheless, there have been developments in our knowledge of the capabilities of the actuators for sawtooth control in ITER even if the operational scope required to avoid NTMs is presently undefined. For instance, the electron cyclotron current drive profiles that can be expected from both the equatorial launcher and the upper launchers have been the subject of much investigation [138, 186–188]. Through EC ray-tracing calculations, the change in the current profile, and subsequently the change in the magnetic shear at the $q = 1$ surface has been determined. These predictions for the ECCD have allowed ASTRA simulations which include the effect of the fusion-born α particles according to reference [22, 99] to assess the sawtooth stability in ITER. It has been predicted that a combination of 13.3MW of co-ECCD from the equatorial launcher and 6.7MW from the upper launcher would be able to reduce the sawtooth period by 30%, or increase it by 50% with a deposition inside or outside $q = 1$ respectively. The fast ion distribution function arising from both on-axis and off-axis negative-ion neutral beam injection has also been computed [189] using the TRANSP code [190], and the effect of the energetic ions on sawtooth stability has been computed [24]. The N-NBI ions are found to be strongly stabilising to the internal kink, and can only incur destabilisation if the $q = 1$ radius is inside $r = 0.2a$. Finally, whilst numerical modelling of the ICCD expected using ^3He minority schemes in ITER predicts the maximum driven current density to be only 0.2-0.5% of the plasma current density and insufficient for any significant modification to the magnetic shear profile [178], an assessment of the kinetic effects anticipated in ITER is underway [191].

In order to simulate the effect of these actuators on sawtooth stability, detailed transport modelling must be coupled to sophisticated fluid-kinetic models to incorporate the effects of the energetic ions rigorously. Although the partial reconnection crash trigger model outlined in section 2.5 is certainly incomplete, it has had notable success in modelling sawtooth behaviour in various devices [101, 103–105, 170], giving greater credence to its application for ITER. Equation 9 indicates that ρ/r_1 must be greater than $\delta W/s_1$ for a sawtooth crash to occur, notwithstanding various normalisation coefficients. However, in ITER the poloidal Larmor radius will be small, which combined with the fact that the baseline operating scenario predicts the $q = 1$ surface to be near mid-radius, means that $\delta W/s_1$ will need to be very small; indeed, much smaller than in present sawtooth control experiments. However, the additional complication of a sizeable population of fusion-born α particles in burning plasmas means that δW is likely to be very large [23, 24] due to the fast trapped ion stabilisation mechanism outlined in

section 2.1.1. This means that the requirement for the change in the magnetic shear is likely to be challenging, and may be ultimately unobtainable without a reduction in the potential energy of the internal kink mode. That said, the linear stability threshold model upon which the modelling to assess the effect of ECCD is based, does not capture all of the dynamics of this process so improvements in our predictive capabilities may lead to more positive assessments. Future experiments will also seek to assess the capability of ECCD to affect sawtooth behaviour in the presence of a strongly-stabilising population of very energetic ions. Due to the inherent uncertainties in the numerical predictions, it is prudent that a combination of both ICRH and ECCD be considered to control the sawteeth in ITER. In any case, it will be necessary to have real-time control of these actuators because of both the uncertainties in the control parameters (launcher aiming, ray-tracing, RF frequency) and the equilibrium (plasma position, q profile etc) and the acute sensitivity of the radial location of the heating or current drive with respect to the rational surface, as highlighted in sections 3 and 5.

An alternative approach to controlling sawteeth which has been recently neglected is to deliberately maximise the sawtooth period. This was considered the most desirable route to sawtooth amelioration in the original ITER Physics Basis [8], and was only superseded by destabilising control tools as anxiety grew about the ramifications of triggering performance-degrading NTMs and due to the need for frequent expulsion of the on-axis accumulation of higher- Z impurities that would otherwise cause degradation of energy confinement due to impurity radiation. Long sawtooth periods are naturally achieved by applying early heating during the current ramp-up phase to increase the conductivity and so slow down the current penetration. Combining this with achieving early ignition will further stabilise the sawteeth due to the α particle stabilisation. ICRH could then be used as an ancillary control tool, with core heating providing a further population of strongly stabilising fast ions. Furthermore, in order to meet the $Q = 10$ goal of ITER baseline scenario, it is desirable to turn off the ECRH power whenever it is not being actively used for mode control. Thus, rather than being constantly required to modify the shear at $q = 1$, an alternative could be envisaged whereby fast ions are used to deliberately stabilise the sawteeth, and before each crash the ECCD is pre-emptively applied near the $q = 2$ surface to stabilise the ensuing NTM [192].

The final approach to dealing with sawteeth is to avoid them all together; Advanced Tokamak scenarios [27–31, 193, 194] represent an attractive way to operate future fusion power plant devices, since they aim to maximise the non-inductive bootstrap current by operating at high plasma pressure and low plasma current. At the same time, the safety factor is above one everywhere, so the plasma is always stable to sawteeth. Whilst the q -profile optimised for stability necessarily operates in a regime which is predicted to be stable to resistive internal instabilities, the absence of such MHD reconnection could result in a deleterious accumulation of helium ash in the plasma core. One possible solution could be using central ECRH deposition since this has been observed to suppress impurity accumulation by increasing the anomalous diffusion and by flattening the profile of the main plasma density which reduces neoclassical inward convection for

the impurities [195, 196].

7. Summary

In recent years there has been considerable progress in both the theoretical understanding of sawtooth control and the experimental implementation of control schemes. It has been shown that both energetic ions and plasma rotation can have a significant effect on the stability of the internal kink mode, thought to underlie the sawtooth phenomenon. As well as the established stabilising effect of trapped fast particles, it has recently been shown that passing fast ions with a large effective orbit width also strongly influence sawtooth stability, due to the radial drift excursion of the energetic ions distributed asymmetrically in the velocity parallel to the magnetic field. When these effects are combined, numerical modelling has been able to explicate the sawtooth behaviour observed with different heating and current drive actuators in a number of tokamaks.

There have also been notable advances in experimental control techniques. Recent results exhibiting destabilisation of sawteeth by steerable electron cyclotron resonance heating (ECRH) have included real-time feedback schemes and robust electron cyclotron current drive (ECCD) control despite the presence of energetic ions in the plasma core. Dramatic changes in sawtooth stability can also be achieved by the application of off-axis ICRH through both changes to the magnetic shear, and perhaps dominantly, through establishing a strong radial gradient in the passing fast ion population just outside the $q = 1$ surface. ICRH has been shown to control sawteeth due to kinetic effects even under conditions where the modification to the magnetic shear is minimised.

Whilst the present explanation of the physics of sawtooth oscillations remains incomplete, various robust control schemes have been established and are now well understood. Consequently, there is reasonable confidence that a combination of sophisticated numerical modelling and further tokamak experiments will establish the requirements of sawtooth control actuators in ITER and ultimately lead to the refinement of a strategy for sawtooth control in burning plasmas.

Acknowledgments

I would like to acknowledge the collaborative spirit of all the authors who have allowed reproduction of their figures. I am also indebted to Dr J Graves, Dr A Kirk, Dr T Hender, Dr S Saarelma, Dr R Dendy, Dr A Thyagaraja, Dr J Hastie and Dr C Gimblett for kindly proof-reading this article and suggesting a number of improvements. This work was funded by the United Kingdom Engineering and Physical Sciences Research Council under grant EP/G003955 and the European Communities under the contract of Association between EURATOM and CCFE. The views and opinions expressed herein do not necessarily reflect those of the European Commission.

References

- [1] Hastie RJ 1998 *Astrophysics and Space Science* **256** 177
- [2] Wesson J 1997 'Tokamaks' (Oxford Science)
- [3] Friedberg JP 1987 'Ideal Magnetohydrodynamics' (Plenum Press)
- [4] Von Goeler S, Stodiek W and Sauthoff N 1974 *Phys. Rev. Letters* **33** 1201
- [5] Park HK *et al* 2006 *Phys. Rev. Lett.* **96** 195003
- [6] Park HK *et al* 2006 *Phys. Rev. Lett.* **96** 195004
- [7] Furno I *et al* 2001 *Nucl. Fusion* **41** 403
- [8] ITER Physics Basis 2007 *Nucl. Fusion* **47** S1
- [9] Nave M F F *et al* 2003 *Nucl. Fusion* **43** 1204
- [10] Campbell DJ *et al* 1988 *Phys. Rev. Lett.* **60** 2148
- [11] La Haye RJ *et al* 1997 *Proc. 24th Eur. Conf. Berchtesgarden* Vol 21A Part III, European Physical Society, Geneva 1121-1244
- [12] Sauter O *et al* 2002 *Phys. Rev. Lett.* **88** 105001
- [13] Gude A, Günter S, Maraschek M and Zohm H 2002 *Nucl. Fusion* **42** 833
- [14] Buttery RJ *et al* 2004 *Nucl. Fusion* **44** 678
- [15] Buttery RJ *et al* 2004 *20th IAEA Fusion Energy Conference, Villamoura EX/7-1*
- [16] Buttery RJ *et al* 2003 *Nucl. Fusion* **43** 69
- [17] Westerhof E *et al* 2006 *Proc 14th Joint Workshop on Electron Cyclotron Emission and Electron Cyclotron Heating* (Santorini, Greece) (Heliotos Conferences Ltd) 38
- [18] Nave, MFF *et al* 1995 *Nucl. Fusion* **35** 509
- [19] La Haye RJ 2006 *Phys. Plasmas* **13** 055501
- [20] Sauter O *et al* 1997 *Phys. Plasmas* **4** 1654
- [21] Zohm H 2001 *Phys. Plasmas* **8** 2009
- [22] Porcelli F, Boucher D and Rosenbluth M 1996 *Plasma Phys. Control. Fusion* **38** 2163
- [23] Hu B, Betti R and Manickam J 2006 *Phys. Plasmas* **13** 112505
- [24] Chapman IT *et al* 2007 *Plasma Phys. Control. Fusion* **49** B385
- [25] Mantsinen MJ *et al* 2002 *Phys. Rev. Lett.* **88** 105002
- [26] Mayoral ML *et al* 2004 *Phys. Plasmas* **11** 2607
- [27] Joffrin E, 2007 *Plasma Phys. Control. Fusion* **49** B629
- [28] Doyle EJ *et al*, 2006 *Plasma Phys. Control. Fusion* **48** B39
- [29] Taylor TS 1997 *Plasma Phys. Control. Fusion* **39** B47
- [30] Sips ACC *et al*, 2005 *Plasma Phys. Control. Fusion* **47** A19
- [31] Joffrin E, 2005 *Nucl. Fusion* **45** 626
- [32] Hastie RJ *et al* 1987 *Phys. Fluids* **30** 1756
- [33] Jacquinot J *et al* 1986 in *Plasma Phys. Control. Nucl. Fus. Res.* **1** 449
- [34] Start D *et al* 1987 *Proc 29th Annual Meeting of APS Division of Plasma Physics, San Diego* **159** 286
- [35] Nave MFF *et al* 2002 *Nucl. Fusion* **42** 281
- [36] Chen L, White RB and Rosenbluth MN 1984 *Phys. Rev. Lett.* **52** 1122
- [37] McGuire K *et al* 1983 *Phys. Rev. Lett.* **50** 891
- [38] White RB, Rutherford P, Colestock P and Bussac M 1988 *Phys. Rev. Lett.* **60** 2038
- [39] White RB, Bussac M and Romanelli F 1989 *Phys. Rev. Lett.* **62** 539
- [40] Coppi B *et al* 1989 *Phys. Rev. Lett.* **63** 2733
- [41] Kruskal M and Oberman C 1958 *Phys. Fluids* **1** 275
- [42] Antonsen T, Lane B and Ramos J 1981 *Phys. Fluids* **24** 1465
- [43] Fogaccia G and Romanelli F 1995 *Phys. Plasmas* **2** 227
- [44] Hastie RJ and Hender TC 1988 *Nucl. Fusion* **28** 585
- [45] Porcelli F 1991 *Plasma Phys. Control. Fusion* **33** 1601
- [46] Van Dam J, Rosenbluth M and Lee Y 1989 *Phys. Rev. Lett.* **62** 539

- [47] Northrop T and Teller E 1960 *Phys. Rev. Lett.* **117** 215
- [48] Graves JP, Sauter O and Gorelenkov N 2003 *Phys. Plasmas* **10** 1034
- [49] Briezman B, Candy J, Porcelli F and Berk H 1998 *Phys. Plasmas* **5** 2326
- [50] Porcelli F, Stankiewicz R, Kerner W and Berk H 1994 *Phys. Plasmas* **1** 470
- [51] Porcelli F *et al* 1990 *15th EPS Conference on Control. Fusion and Plasma Heating, Dubrovnik* **12B/1** 377
- [52] Graves JP, Hastie RJ and Hopcraft KI 2000 *Plasma Phys. Control. Fusion* **42** 1049
- [53] Graves JP 2005 *Phys. Plasmas* **12** 090908
- [54] Rice JE *et al* 2007 *Nucl. Fusion* **47** 1618
- [55] Halpern FD, Kritz AH, Bateman G, Pankin AY, Budny RV and McCune DC 2008 *Phys. Plasmas* **15** 062505
- [56] Betti R and Friedberg J 1993 *Phys. Rev. Lett.* **70** 3428
- [57] Wang S, Ozeki T and Tobita K 2002 *Phys. Rev. Lett.* **88** 105004
- [58] Graves JP 2004 *Phys. Rev. Letters* **92** 185003
- [59] Kolesnichenko Ya, Marchenko VS and White RB 2005 *Phys. Plasmas* **12** 022501
- [60] Graves JP, Chapman IT, Coda S, Johnson T and Koslowski HR 2009 *accepted Phys. Plasmas*
- [61] Graves JP *et al* 2010 *Nucl. Fusion.* **50** 052002
- [62] Graves JP, Chapman IT, Coda S, Eriksson LG and Johnson T 2009 *Phys. Rev. Lett.* **102** 065005
- [63] Akers RJ *et al* 2002 *Nucl. Fusion* **42** 122
- [64] Waelbroeck FL 1996 *Phys. Plasmas* **3** 1047
- [65] Wahlberg C and Bondeson A 2000 *Phys. Plasmas* **7** 923
- [66] Wahlberg C 2005 *Plasma Phys. Control. Fusion* **47** 757
- [67] Kleva R and Guzdar P 2002 *Phys. Plasmas* **9** 3013
- [68] Chapman IT, Hender TC, Saarelma S, Sharapov SE, Akers RJ and Conway NJ 2006 *Nucl. Fusion* **46** 1009
- [69] Wahlberg C, Chapman IT and Graves JP 2009 *Phys. Plasmas* **16** 112512
- [70] Chapman IT, Graves JP and Wahlberg C 2010 *Nucl. Fusion* **50** 025018
- [71] Cowley SC, Kulsrud RM and Hahm TS 1986 *Phys. Fluids* **29** 3230
- [72] Pegoraro F, Porcelli F and Schep TJ 1989 *Phys. Fluids B* **1** 364
- [73] Drake JF, Antonsen TM, Hassam AB and Gladd NT 1983 *Phys. Fluids* **26** 2509
- [74] Migliuolo S 1993 *Nucl. Fusion* **33** 1721
- [75] ITER Physics Basis 1999 *Nucl. Fusion* **39** 2137
- [76] Shafranov VD 1970 *Sov. Phys. Tech. Phys.* **15** 175
- [77] Bussac MN *et al* 1975 *Phys. Rev. Lett.* **35** 1638
- [78] Coppi B, Galvao R, Pellat R, Rosenbluth MN and Rutherford PH 1976 *Sov. J. Plasma Phys.* **2** 533
- [79] Kadomtsev BB 1976 *Sov. J. Plasma Phys.* **1** 389
- [80] Edwards AW *et al* 1986 *Phys. Rev. Letters* **57** 210
- [81] Dubois, MA and Party, D and Pochelon, A 1980 *Nucl Fusion* **20** 1355
- [82] Soltwisch H and Stodiek W 1987 *Proc. 29th Annual Meeting of APS Division of Plasma Physics, San Diego*
- [83] Blum J *et al* 1990 *Nucl. Fusion* **30** 1475
- [84] O'Rourke, J 1991 *Plasma Phys. Control. Fusion* **33** 289
- [85] Yamada M *et al* 1994 *Phys. Plasmas* **1** 3269
- [86] Campbell DJ *et al* 1986 *Phys. Rev. Lett.* **57** 210
- [87] Bussac, MN and Edery, D and Pellat, R and Soule, JL 1976 *Plasma Phys. and Controlled Nucl. Fusion Research (IAEA Vienna)* **1** 607
- [88] Ara G *et al* 1978 *Annals of Physics* **112** 443
- [89] Migliuolo, S and Pegoraro, F and Porcelli, F 1991 *Phys. Fluids B* **3** 1338
- [90] Ottaviani, M and Porcelli, F 1993 *Phys. Rev. Lett.* **71** 3802
- [91] Lichtenberg, AJ and Itoh, K and Itoh, SI and Fukayama, A 1992 *Nucl. Fusion* **32** 495

- [92] Igochine V, Dumbrajs O, Zohm H and Flaws A 2007 *Nucl. Fusion* **47** 23
- [93] Wesson J *et al* 1986 *Plasma Phys. Control. Fusion* **28** 243
- [94] Gimblett CG and Hastie RJ 1994 *Plasma Phys. Control. Fusion* **36** 1439
- [95] Park W *et al* 1995 *Phys. Rev. Lett.* **75** 1763
- [96] Nishimura Y, Callen JD and Hegna CC 1999 *Phys. Plasmas* **6** 4685
- [97] Chu TK 1988 *Nucl. Fusion* **28** 1109
- [98] Bateman G, Nguyen CN, Kritz AH and Porcelli F 2006 *Phys. Plasmas* **13** 072505
- [99] Sauter O *et al* 1998 *Theory of Fusion Plasmas, Proc Joint Varenna-Lausanne International Workshop, Varenna (AIP)* p403
- [100] Martynov, An and Graves, JP and Sauter, O 2005 *Plasma Phys. Control. Fusion* **47** 1743
- [101] Levinton FM *et al* 1994 *Phys. Rev. Lett.* **72** 2895
- [102] Porcelli F 1991 *Phys. Rev. Lett.* **66** 425
- [103] Angioni C *et al* 2002 *Plasma Phys. Control. Fusion* **44** 205
- [104] Angioni C, Goodman T, Henderson M and Sauter O 2003 *Nucl. Fusion* **43** 455
- [105] Choi M *et al* 2007 *Phys. Plasmas* **14** 112517
- [106] Bobrovskii G *et al* 1987 *Sov. J. Plasma Phys.* **13** 665
- [107] Kuvshinov BN and Savrukhn PV 1990 *Sov. J. Plasma Phys.* **16** 353
- [108] Hanada K *et al* 1991 *Phys. Rev. Lett.* **66** 1974
- [109] Snider RT *et al* 1989 *Phys. Fluids B* **1** 404
- [110] Hanada K *et al* 1992 *Phys. Fluids B* **4** 2675
- [111] Westerhof E *et al* 2003 *Nucl. Fusion* **43** 1371
- [112] Ikeda Y *et al* 2002 *Nucl. Fusion* **42** 375
- [113] Muck A *et al* 2002 *29th EPS Conference on Controlled Fusion and Plasma Physics, Montreux* **26B** P1.037
- [114] Bhatnagar VP *et al* 1994 *Nucl. Fusion* **34** 1579
- [115] Start DFH *et al* 1992 *Proc. Int. Conf. Plasma Physics (Innsbruck)* vol 16C Part II (Geneva: European Physical Society) p1521
- [116] Fisch NJ 1987 *Rev. Mod. Phys.* **59** 175
- [117] Hellsten T, Carlsson J and Eriksson L-G 1995 *Phys. Rev. Lett.* **74** 3612
- [118] Carlsson J, Hellsten T and Hedin J 1998 *Phys. Plasmas* **5** 2885
- [119] Mück A, Goodman TP, Maraschek M, Pereverez G, Ryter F and Zohm H 2005 *Plasma Phys. Control Fusion* **47** 1633
- [120] Pinsker RI *et al* 2003 *Bull. Am. Phys. Soc.* **48** 128
- [121] Sauter O *et al* 2001 *Phys. Plasmas* **8** 2199
- [122] Henderson MA *et al* 2001 *Fus. Eng. Des.* **53** 241
- [123] Zohm H *et al* 2003 *Nucl. Fusion* **43** 1570
- [124] Manini A *et al* 2005 *32nd EPS Conference on Plasma Physics, Tarragona, Spain* **29C** P4.073
- [125] Maraschek M *et al* 2005 *Nucl. Fusion* **45** 1369
- [126] Manini A *et al* 2006 *14th Joint Workshop on ECE and ECRH, Santorini*
- [127] Goodman TP *et al* 2003 *Nucl. Fusion* **43** 1619
- [128] Graves JP *et al* 2005 *Plasma Phys. Control. Fusion* **47** B121
- [129] Isayama A *et al* 2002 *J. Plasma Fus. Res. Series* **5** 324
- [130] Lennholm M *et al* 2007 *17th Top. Conf. on Radio Frequency Power in Plasmas* **933** 401
- [131] Cirant S *et al* 1998 *17th IAEA Fusion Energy Conference, Yokohama* CDP/07
- [132] Asakawa M *et al* 1998 *17th IAEA Fusion Energy Conference, Yokohama* CDP/06
- [133] Lennholm M *et al* 2009 *Phys. Rev. Lett.* **102** 115004
- [134] Pietrzyk ZA *et al* 1999 *Nucl. Fusion* **39** 587
- [135] Reimerdes H *et al* 2000 *Plasma Phys. Control. Fusion* **42** 629
- [136] Polevoi A, Medvedev S, Mukhovatov V, Kukushkin A, Murakami Y, Shimada M and Ivanov A, 2002 "ITER Confinement and Stability Modelling", *J. Plasma Fusion Res.* **5**
- [137] Merkulov A *et al* 2004 *Theory of Fusion Plasmas, Joint Varenna-Lausanne Theory Workshop*

- p279
- [138] Zucca C *et al* 2008 *Theory of Fusion Plasmas, Joint Varenna-Lausanne Theory Conference* **1069** 361
 - [139] Zucca C 2009 *PhD Thesis No 4360, EPFL, Lausanne* “Modeling and control of the current density profile in tokamaks and its relation to electron transport”
 - [140] Paley JI *et al* 2009 *Nucl. Fusion* **49** 085017
 - [141] Paley JI *et al* 2009 *Plasma Phys. Control. Fusion* **51** 055010
 - [142] Lennholm M *et al* 2009 *Fus. Sci. Tech.* **55** 45
 - [143] Paley JI, Felici F, Coda S and Goodman TP 2009 *Plasma Phys. Control. Fusion* **51** 124041
 - [144] Igochine VG *et al* 2010 *In prep for Nucl. Fusion*
 - [145] Liu Yi *et al* 2010 *Private Communication*
 - [146] Ekedahl A *et al* 1998 *Nucl. Fusion* **38** 1397
 - [147] Söldner FX *et al* 1994 *Nucl. Fusion* **34** 985
 - [148] Chu TK *et al* 1986 *Nucl. Fusion* **26** 666
 - [149] Wukitch S *et al* 2005 *Phys. Plasmas* **12** 056104
 - [150] Parisot A *et al* 2007 *Plasma Phys. Control. Fusion* **49** 219
 - [151] Thyagaraja A, Hazeltine RD and Aydemir AY 1992 *Phys. Fluids B* **4** 2733
 - [152] Mao JS *et al* 2005 *Plasma Science Technology* **7** 2816
 - [153] Mao JS *et al* 2002 *Chinese Phys. Lett.* **19** 220
 - [154] Kramer G *et al* 2000 *Nucl. Fusion* **40** 1383
 - [155] Nave MFF *et al* 2006 *Phys. Plasmas* **13** 014503
 - [156] Chapman IT, Pinches SD, Graves JP, Appel LC, Hastie RJ, Hender TC, Saarelma S, Sharapov SE and Voitsekhovitch I 2007 *Phys. Plasmas* **14** 070703
 - [157] Chapman IT, Pinches SD, Koslowski HR, Liang Y, Kramer-Flecken A and de Bock M 2008 *Nucl. Fusion* **48** 035004
 - [158] Chapman IT, Huysmans GTA, Mikhailovskii AB and Sharapov SE 2006 *Phys. Plasmas* **13** 062511
 - [159] Pinches SD, Appel LC, Candy J, Sharapov SE, Berk HL, Borba D, Breizman BN, Hender TC, Hopcraft KI, Huysmans GTA and Kerner W, *Comput. Phys. Commun.*, **111**, 133 (1998)
 - [160] Chapman IT *et al* 2008 *Plasma Phys. Control. Fusion* **50** 045006
 - [161] Chapman IT *et al* 2009 *Nucl. Fusion* **49** 035006
 - [162] Chapman IT *et al* 2009 *Phys. Plasmas* **16** 072506
 - [163] Phillips CK *et al* 1992 *Phys. Fluids B* **4** 2155
 - [164] Eriksson L-G *et al* 1998 *Phys. Rev. Lett.* **81** 1231
 - [165] Graves JP *et al* 2000 *Phys. Rev. Lett.* **84** 1204
 - [166] McClements KG *et al* 1996 *Phys. Plasmas* **3** 2994
 - [167] Westerhof E *et al* 2002 *Nucl. Fusion* **42** 1324
 - [168] Eriksson L-G *et al* 2004 *Phys. Rev. Letters* **92** 235004
 - [169] Eriksson L-G *et al* 2006 *Nucl. Fusion* **46** S951
 - [170] Mantsinen M *et al* 2002 *Plasma Phys. Control. Fusion* **44** 1521
 - [171] Mantsinen M *et al* 2002 *Phys. Rev. Lett.* **91** 115004
 - [172] Coda S *et al* 2007 *Proc 34th EPS Conf. on Plasma Physics (Warsaw, Poland)* P5.130
 - [173] Eriksson L-G, Hellsten T and Willen U 1993 *Nucl. Fusion* **33** 1037
 - [174] Carlsson J, Eriksson L-G and Hellsten T 1994 *Theory of Fusion Plasmas, Joint Varenna-Lausanne International Workshop* p351
 - [175] Dendy RO *et al* 1995 *Phys. Plasmas* **2** 1623
 - [176] Graves JP, Cooper WA, Coda S, Eriksson LG and Johnson T 2006 *Theory of Fusion Plasmas, Joint Varenna-Lausanne International Workshop* p350
 - [177] Hedin J *et al* 2002 *Nucl. Fusion* **42** 527
 - [178] Laxåback M and Hellsten T 2005 *Nucl. Fusion* **45** 1510
 - [179] Lennholm M 2009 *Private Communication*
 - [180] Jardin SC, Bell MG and Pomphrey N 1993 *Nucl. Fusion* **33** 371

- [181] Bateman G *et al* 1998 *Phys. Plasmas* **5** 2355
- [182] Waltz R *et al* 1997 *Phys Plasmas* **4** 2482
- [183] Onjun T and Pianroj Y 2009 *Nucl. Fusion* **49** 075003
- [184] Budny RV *et al* 2008 *Nucl. Fusion* **48** 075005
- [185] Chapman IT *et al* 2010 *sub Nucl. Fusion*
- [186] Henderson M *et al* 2005 *3rd IAEA TM on ECRH Physics and Technology in ITER (Como, Italy)*
p 143
- [187] Houlberg WA *et al* 2005 *Nucl. Fusion* **45** 1309
- [188] Maruschenko NB, Maassberg H and Turkin Y 2008 *Nucl. Fusion* **48** 054002
- [189] Budny RV 2002 *Nucl. Fusion* **42** 1383
- [190] Budny RV *et al* 1992 *Nucl. Fusion* **32** 429
- [191] Johnson T, Graves JP 2010 *Private Communication*
- [192] Sauter O, Henderson MA, Ramponi G, Zohm H and Zucca C 2010 *Nucl. Fusion* **52** 025002
- [193] Kessel CE, Manickam J, Rewoldt G and Tang W, 1994 *Phys. Rev. Lett.* **72** 1212
- [194] Becoulet A and Hoang GT, 2008 *Plasma Phys. Control. Fusion* **50** 124055
- [195] Dux R *et al*, 2003 *Journal of Nuclear Materials* **313** 1150
- [196] Neu R *et al*, 2002 *Plasma Phys. Control. Fusion* **44** 811